



**TÉCNICO**  
LISBOA

# **Tumour targeting nanoparticles for fluorescence-guided surgery**

**Inês Santos Pereira Lebre**

Thesis to obtain the Master of Science Degree in

## **Materials Engineering**

Advisor(s)/Supervisor(s): Prof. Carlos Baleizão,  
Prof. José Paulo Farinha

### **Examination Committee**

Chairperson: Prof. Dr. Alberto Ferro

Advisor: Prof. Dr. José Paulo Farinha

Members of the Committee: Prof. Dr. Ermelinda Maços

**October 2021**



# Acknowledgments

To FCT-Portugal and COMPETE/FEDER through funding within projects UIDB/00100/2020 and PTDC/CTM-CTM/32444/2017.

I would like to thank my parents for all the caring and support over all these years. And to my friends and colleagues who helped me during my studies.

Lastly, I want to thank my supervisors and lab colleagues without whom this project would not be possible.



## Abstract

Cancer is one of the deadliest diseases and many tumours have to be surgically removed. To help surgeons during tumour excision, we developed a fluorescent nanoparticles system with affinity to cancer cells to highlight the tumours to be removed.

Silica particles with a fluorescent NIR emitting cyanine dye, based on indocyanine green (FIGS-IST-Dye1) were produced by the Stöber method. The dye has silane groups in its structure, for anchoring into the silica matrix during synthesis.

For targeting the tumours, the NP were surface covered with folate groups since cancer cells over-express folate receptors. Two different functionalization methods were tested. The first is a two-step method, with activation of the nanoparticles, washing and then functionalization. The second is one-step, where all the components are added sequentially during the reaction. The surface coverage with folate was measured by  $^1\text{H}$  NMR, and the two-step method was found to yield the best results.

A photo-degradation test showed that the dye inside the particles has a better photo-stability. Cell viability tests with fibroblast showed that the particles obtained are biocompatible at concentrations below  $100\ \mu\text{g}/\text{mL}$ .

The nanoparticles developed in this work have excellent potential for use in fluorescence guided surgery using current NIR surgical equipment.

**Keywords:** Nanoparticle, Indocyanine Green (ICG), Fluorescence-guided surgery (FGS), Selective targeting, Folic acid



## Resumo

O cancro é uma das doenças com maior mortalidade no mundo e muitos tumores precisam de ser removidos cirurgicamente. Para ajudar os cirurgiões durante a excisão tumoral, desenvolvemos um sistema de nanopartículas fluorescentes com afinidade a células cancerígenas para destacar os tumores enquanto são removidos.

Partículas de sílica com cianina fluorescente emissora de luz infravermelha próxima, à base de indocianina verde (FIGS-IST-Dye1) foram produzidas pelo método de Stöber. O marcador possui grupos silanos na sua estrutura, para ancoragem na matriz de sílica durante a síntese.

Para direcionar as nanopartículas para o tumor, estas foram cobertas à superfície com grupos folato, uma vez que as células cancerígenas têm uma maior expressão de receptores folato. Dois métodos diferentes de funcionalização foram testados. O primeiro, em dois passos, consiste em ativar as partículas, lavar e depois funcionalizar. No segundo, em um passo, introduzimos todos os reagentes sequencialmente durante a reação. A cobertura da superfície com folato foi medida por  $^1\text{H}$  RMN, e o método por dois passos mostrou melhores resultados.

Um teste de foto-degradação mostrou que o marcador dentro das partículas possui uma melhor foto-estabilidade. Testes de viabilidade celular com fibroblastos mostraram que as partículas obtidas são biocompatíveis em concentrações abaixo de  $100 \mu\text{g/mL}$ .

As nanopartículas desenvolvidas neste trabalho têm excelente potencial para uso em cirurgia guiada por fluorescência utilizando equipamentos cirúrgicos de luz infravermelha próxima.

**Keywords:** Nanopartícula, Indocianina verde (ICG), Cirurgia guiada por fluorescência, Diferenciação seletiva, Ácido fólico





# Contents

<b>List of Tables</b>	<b>ix</b>
<b>List of Figures</b>	<b>xi</b>
<b>Acronyms</b>	<b>1</b>
<b>1 Introduction</b>	<b>3</b>
1 Fluorescence Guided Surgery (FGS) . . . . .	3
1.1 Indocyanine green . . . . .	4
1.2 Types of tumour targeting . . . . .	5
1.2.1 Passive Targeting . . . . .	5
1.2.2 Active Targeting . . . . .	6
2 Nanoparticles . . . . .	7
3 Objectives . . . . .	10
<b>2 Experimental Procedure</b>	<b>13</b>
1 Reagents and Solvents . . . . .	13
2 Equipment . . . . .	13
2.1 Centrifuge . . . . .	13
2.2 Dynamic Light Scattering (DLS) . . . . .	13
2.3 Fluorescence Spectroscopy . . . . .	14
2.4 Nuclear Magnetic Resonance (NMR) . . . . .	14
2.5 Transmission Electron Microscopy (TEM) . . . . .	14
2.6 UV/Vis Spectroscopy . . . . .	14
2.7 Microplate Reader . . . . .	14
3 Synthesis of Stöber Silica Nanoparticles . . . . .	15
4 Surface functionalization of Silica Nanoparticles . . . . .	15
4.1 Two Steps Route . . . . .	15
4.2 One step Route . . . . .	16
5 Cell Viability . . . . .	17
<b>3 Results and Discussion</b>	<b>19</b>
1 Synthesis of Silica Nanoparticles . . . . .	19
2 Silica NP Functionalization . . . . .	22
3 Fluorescence Studies . . . . .	25
4 Stability test . . . . .	28
5 Cell Viability . . . . .	29
<b>4 Conclusions</b>	<b>33</b>
<b>Bibliography</b>	<b>34</b>
<b>Appendix</b>	<b>39</b>
A) DLS Correlograms . . . . .	39
B) NMR spectra . . . . .	42



# List of Tables

1.1	Structure and properties of fluorescence probes in medical use . . . . .	4
2.1	Reagents quantities used in the different synthesis. . . . .	15
3.1	Diameter of the SiNP measured by DLS and TEM. . . . .	19
3.2	Zeta Potential in multiple functionalizations. . . . .	23
3.3	Quantification of SiNPs functional groups . . . . .	25
3.4	Cell viability after 1 h of PrestoBlue™ introduction. . . . .	30
3.5	Cell viability after 48 h incubation. . . . .	30



# List of Figures

1.1	Structures of IRDye 800CW (a) and indocyanine green (b). Adapted from [12]. . . . .	5
1.2	Illustration of a passive targeting mechanism . . . . .	6
1.3	Structure of Folic Acid . . . . .	7
1.4	Schematic representation of different types of nanoparticles (NPs) divided into organic, hybrid and inorganic categories . . . . .	8
1.5	Mechanism of hydrolysis of TEOS precursors in base (B:)-catalyzed reactions . . . . .	8
1.6	Mechanism of condensation of TEOS precursors in base (B:)-catalyzed reactions . . . . .	9
1.7	Structure of bis(propyl)triethoxysilane perylenediimide. . . . .	10
1.8	FIGS-IST-Dye1 . . . . .	11
2.2	Schematic representation of functionalization of a SiNP with folic acid via two steps route.	16
2.3	Schematic representation of functionalization of a SiNP with folic acid via one steps route.	16
3.1	Correlograms obtained by DLS for Si3@PDI. . . . .	20
3.2	TEM images from reactions: Si3@PDI (a), Si4@PDI (b), Si5@FIGS (c). . . . .	20
3.3	Reactional mixture of Si5@FIGS synthesis, before centrifugation (a); supernatant obtained in the first wash (b, left) and second wash (b, right); particles Si5@FIGS after washed and dried (c). . . . .	21
3.4	TEM images from reaction: Si6A (a), Si6B (b). . . . .	21
3.5	Schematic representation of functionalization of a SiNP with folic acid via two steps route.	22
3.6	Schematic representation of functionalization of a SiNP with folic acid via one steps route.	23
3.7	Si3@PDI from left to right: before functionalization, functionalized by the two step procedure, functionalized by the one step procedure. . . . .	23
3.8	$^1H$ NMR of non functionalized Si3. . . . .	24
3.9	$^1H$ NMR of Si3-PDI functionalized by the Two Step method, with peaks assignment. . . . .	25
3.10	Normalized fluorescence spectrum of (a) Si3@PDI, functionalized via One Step method in H <sub>2</sub> O and (b) Si4@PDI functionalized via Two Step method in H <sub>2</sub> O. In dashed red, we have excitation curves (em= 580 nm) and at solid black, emission curves (ex=490 nm). In blue we have the spectrum of PDI before synthesis, in toluene. . . . .	26
3.11	Absorption spectrum of free FIGS (red) in methanol, and Si5@FIGS (black). . . . .	26
3.12	Normalized fluorescence spectrum of Si5@FIGS (red) in H <sub>2</sub> O and free FIGS-IST-Dye1 (black) in methanol. Excitation (dashed curves) of the NP measured at 840 nm, and of the free dye at 825 nm. Emission (solid curve) of the NP measured at 680 nm, and of the free dye at 710 nm. . . . .	27
3.13	Emission spectrum of Si5@FIGS with excitation at 550nm. . . . .	27
3.14	Spectrum of the solution obtained after centrifuging the reaction mixture obtained. In red, we have excitation curves (em=650nm) and at black emission (ex=450nm). . . . .	28

3.15	Fluorescence intensity at 800 nm with 680 nm excitation for free dye (a) and Si5@FIGS (b). Red lines are a guide to the eye. . . . .	28
3.16	Fluorescence intensity at 800 nm with 680 nm excitation for free dye (a) and Si5@FIGS (b) with scales adapted for a better visualization. . . . .	29
3.17	96-Well Cell Culture Plate. . . . .	30
3.18	Graphic representation of cell viability after 1h of introduction of particles (red) and after 48h (blue). . . . .	31
1	Correlograms obtained by DLS for Si4@PDI. . . . .	39
2	Correlograms obtained by DLS for Si5@FIGS. . . . .	40
3	Correlograms obtained by DLS for Si6A. . . . .	40
4	Correlograms obtained by DLS for Si6B. . . . .	41
5	<sup>1</sup> H NMR of Si-PDI functionalized by the One Step method. Peak assignment: 8.55, 7.64, 6.80 Folic Acid; 5.17 Trioxane; 4.79 D2O; 3.61, 1.12 Ethanol; 2.55, 1.46, 0.46 APTES. . .	42
6	<sup>1</sup> H NMR of Si4-PDI functionalized by the One Step method. Peak assignment: 8.46, 7.54, 6.70 Folic Acid; 5.12 Trioxane; 4.79 D2O; 3.55, 1.07 Ethanol; 2.46, 1.39, 0.37 APTES. . .	43
7	<sup>1</sup> H NMR of Si5-FIGS-IST-Dye1 functionalized by the Two Step method, with integration ranges represented. Peak assignment: 8.52, 7.54, 6.76 Folic Acid; 5.14 Trioxane; 4.79 D2O; 3.54, 1.08 Ethanol; 2.48, 1.43, 0.39 APTES. . . . .	44

# Acronyms

**APTES** 3-aminopropyl triethoxysilane.

**Ar** Argon.

**DCC** N,N'-Dicyclohexylcarbodiimide.

**DCM** Dichloromethane.

**DLS** Dynamic Light Scattering.

**DMEM** Dulbecco's Modified Eagle's Medium.

**DMF** N,N-Dimethylformamide.

**DMSO** Dimethyl sulfoxide.

**EPR** enhanced permeability and retention.

**FA** Folic Acid.

**FBS** Fetal Bovine Serum.

**FGS** Fluorescence Guided Surgery.

**ICG** Indocyanine Green.

**NH<sub>4</sub>OH** Ammonium hydroxide.

**NIR** Near Infrared.

**NMR** Nuclear Magnetic Resonance.

**NP** nanoparticles.

**PB** PrestoBlue™.

**PDI** Perylenediimide.

**SiNPs** Silica Nanoparticles.

**TEM** Transmission Electron Microscopy.

**TEOS** tetraethyl orthosilicate.

**WHO** World Health Organization.





# Chapter 1

## Introduction

According to the World Health Organization (WHO), cancer is the second most common cause of death, being responsible, on a global scale, for about 10 million deaths per year. This disease is characterized by an uncontrolled development of cells that lost the ability to function in a normal way, due to damage in the DNA. Cancer cells keep dividing, do not die when they should and do not mature to develop a specific function. This out of control multiplication leads to a mass called a tumour. As the tumour grows the nutrients and oxygen needs increase, and it signals the body to form new blood vessels, in a process called angiogenesis. This also facilitates the spread of cancer to other locations, through the bloodstream or lymphatic system, creating metastasis. The earlier it is detected and treated, the higher the cure rates. The treatment is evidence-selected, case by case, with options including surgery, radiotherapy, chemotherapy and adjuvant medicines. [1, 2]

### 1 Fluorescence Guided Surgery (FGS)

If all the cancer cells are removed or killed, cancer may be considered in remission or cured. Nonetheless, if even a small number of cells remain, these can multiply again and originate a new tumour, called a recurrence. [2] During surgical tumours resection it is crucial to obtain negative margins to prevent future recurrences. This means that no cancer cells are found by the pathologist when examining the outer edge of the removed tissue. [3] This procedure is dependent on the surgeon skills and judgement, combined with preoperative imaging research and intraoperative histopathological analysis of removed tissue sections. However, this leads to positive margins, in 50-70 % of curative surgeries, with cancer cells still found at the edge of the tissue. [4, 5]

To help the surgeons, real-time imaging techniques can be used to improve the perception of tumour cells and therefore minimize the recurrence rates. These techniques can, for example, use fluorescent probes and optical imaging devices.

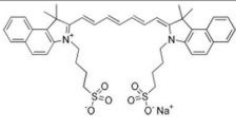
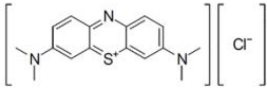
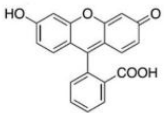
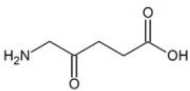
A fluorescent probe or fluorophore is a molecule that absorbs and emits light in specific wavelengths. Fluorophores are divided into three main groups: i) organic dyes and the counterparts that can be obtained through synthetic chemistry, which have the advantage of having a small size compared to the biological fluorophores; ii) biological fluorophores (fluorescent proteins), that can be introduced into live cells or expressed by the cells; iii) functionalized quantum dots, are semiconductor nanoparticles, and the optical properties differ not only based on the composition but also on the particle size and shape (these have been increasingly used in biological research since they can be coated with different molecules such as proteins, but must presents high levels of toxicity). [6]

For fluorescence guided surgery (FGS), one needs high tissue penetration and minimal light scattering. In this case, near infrared (NIR) is the best option, being the optimal range between 700-900

nm, due to the reduced light scattering compared to the visible light, combined with high tissue penetration, minimal biological auto-fluorescence and absorption. Considering that the light below 700 nm is absorbed by the tissues and endogenous molecules and above 900 by lipids and water, that range ensures the best tissue penetration. [7, 8]

Table 1.1 compiles the dyes already in use in FGS: indocyanine green (ICG), methylene blue (MB), fluorescein, and 5-Aminolevulinic acid (5-ALA). We will describe ICG in more detail in the next section. Methylene blue (MB) is a NIR fluorescent aromatic fluorescent compound, mostly used to identify breast cancer, neuroendocrine tumours and sentinel lymph node mapping. It is approved by the FDA and considered safe, but with potential to induce cardiac arrhythmias, coronary vasoconstriction, decreased cardiac output, decreased renal blood flow and mesenteric blood flow, and increased pulmonary vascular pressure. [8] Fluorescein, first used in 1947, is an organic fluorescent dye visible by naked eye or with a yellow filter at low doses, used for ophthalmology and brain tumour visualization. [4, 8] 5-ALA is a special case, since it is not fluorescent by itself, but induces the synthesis and accumulation of protoporphyrin IX (PpIX), a fluorescent molecule, in the epithelial and neoplastic tissues. The emission and excitation peaks are dependent on the application site pH. It is mainly used for malignant glioma cells (brain and spinal cords), and for bladder and prostate cancer. [4, 8]

Table 1.1: Structure and properties of fluorescence probes in medical use. Reprinted from [4].

FDA approved fluorescence probe	Molecular structure	Excitation wavelength (nm)	Emission wavelength(nm)
Indocyanine green (ICG)		780	820
Methylene blue (MB)		670	690
Fluorescein sodium		494	512
5-Aminolevulinic acid (5-ALA)		380–440	620 (alkaline pH); 634 (acidic pH)

## 1.1 Indocyanine green

Indocyanine Green is a fluorescent marker and one of the most used in NIR Fluorescence Guided Surgery (FGS) (fig 1.1 a)). It was the first NIR fluorophore approved by the FDA for *in vivo* use in humans. [4] Produced for the first time in 1955, by Kodak Laboratories, it is a water-soluble molecule with a low allergic reaction rate used in various types of cancers resection surgery. The dye can bind to proteins without loss of its fluorescence properties. [4, 8] Even though it has no specific affinity for cancer cells, ICG binds to plasma albumin, remaining in circulation, and allows the lymphatic mapping and a liver and biliary structure evaluation since it is excreted by the hepatic system. [5, 8]

Nevertheless, ICG has poor photostability, especially in aqueous environments, and poor hydrolytic stability, which implies time-limited surgeries, not advised when trying to achieve surgical resection such as a total peritoneal cytoreduction. [9] Its half-life is relatively short, between 150s and half an hour. This can be solved by injecting a higher amount of dye, but with possible toxicity or excretion

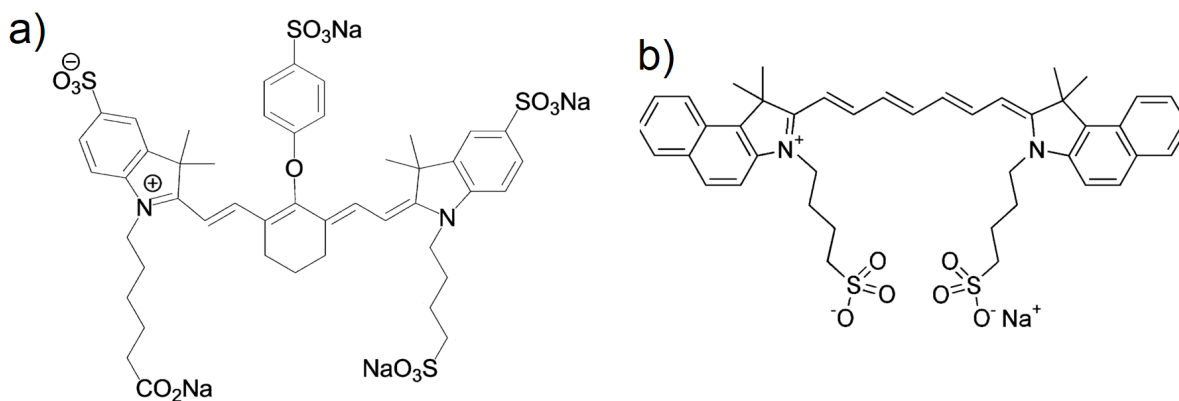


Figure 1.1: Structures of IRDye 800CW (a) and indocyanine green (b). Adapted from [12].

problems. When measuring the signal to background ratio (SBR), a value higher than 5 ensures a reliable identification of the object. In ICG, the SBR is 2 meaning the fluorescent contrast to the tissue is poor. [9, 10] IRDye800CW is marker from the cyanine family that has been grabbing attention in the last years in a development of a general-purpose NIR that can be conjugated with other molecules for targeting (fig 1.1b)). [11] It is still not US-FDA approved for FGS but is in clinical trials for pancreatic and colorectal cancer. [8] In PBS, the maximum absorbance was 774 nm and the maximum emission was 789 nm, with an improved quantum yield (from 0.9 % in ICG to 3.3 % in IRDye800CW, in aqueous medium). [12, 13] In studies with IRDye800CW, there were no signs of toxic effects in the animals tested, being the maximum concentration evaluated 20 mg/kg. Nevertheless, the uptake in the popliteal lymph nodes varies according to the administration procedure (less via intravenous than intradermal injection). [12] One drawback found was colouring at the injection site or at the dorsal surface for several days, when administered, respectively, by intravenous or intradermal injections. The clearance is expected to happen within 24 h. After 15 days there were no clinical relevant modifications. [14, 12]

## 1.2 Types of tumour targeting

Targeting allows a dye that is injected or delivered to the body to accumulate at the desired location and allow its visualization. Selective targeting leads to an adequate biodistribution, minimizing toxicity and protecting the dye from the multiple threats in the body and therefore increasing the efficiency and minimizing side effects. [4]

### 1.2.1 Passive Targeting

Passive targeting is a natural body reaction toward macromolecules and nanoparticles, which makes use of vascularization differences for distribution and targeting of the cancerous tissue. This phenomenon is mainly explained by the enhanced permeability and retention (EPR) effect (Fig.1.2). Surrounding the tumour there is excessive vascularization and higher permeability due to large gap junctions (100-600 nm). Larger molecules or nanoparticles, especially with diameters between 30-200 nm, face difficulties in penetrating the endothelium of normal blood vessels. However, they easily can penetrate tumour vessels. Furthermore, there is a lack of lymphatic drainage in tumours that prevents the accumulation of macromolecules in healthy tissue, leading to a perfect environment for retention. EPR can be used to label tumours with a fluorescent dye, by attaching the dye to macromolecules or nanoparticles. [15, 16]

According to some studies, the range of 30-50 nm is the optimum for cellular uptake, interacting with

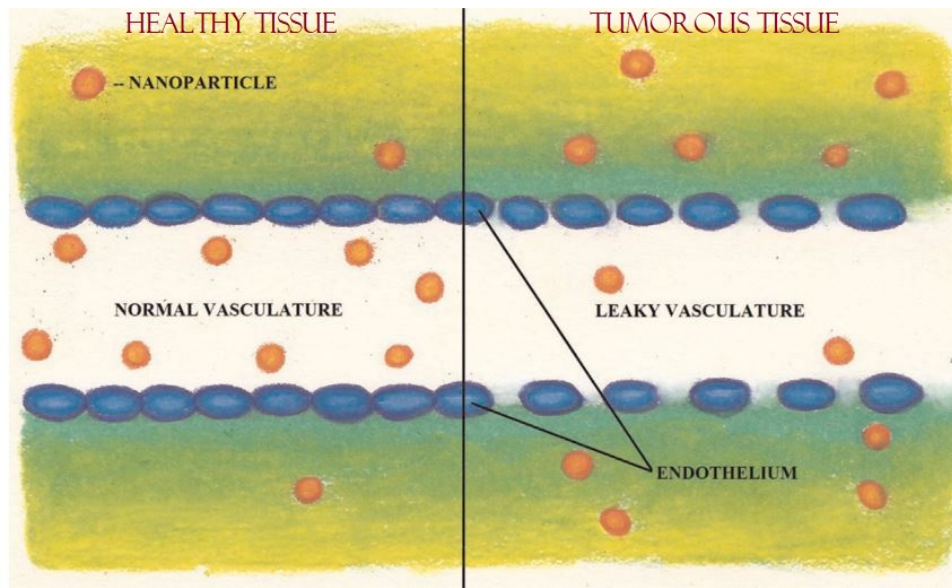


Figure 1.2: Illustration of passive targeting based on the difference between healthy and tumour tissue, that leads to a higher accumulation of nanoparticles on the tumour. Adapted from [16].

the plasma membrane receptors to be endocytosed in a receptor-mediated process or by macropinocytosis. Different sizes are also uptaken, using other endocytosis processes, up to a maximum diameter of around  $3 \mu m$ , but bigger NPs are more easily eliminated by the reticuloendothelial system and smaller ones do not activate the membrane receptors and proteins. Direct application of a marker onto the tumour, avoiding systemic circulation, is also an option. [17]

### 1.2.2 Active Targeting

This form of targeting uses specific receptors and endocytosis systems to deliver the desired molecule at the site. The targets can be cell-surface carbohydrates (using proteins to bind to the carbohydrates), cellular antigens (using antibodies that connect to the antigens on tumour cells) or cell-surface receptors (using ligand that bind to receptors on the surface of cells). [15, 16]

One way to achieve active targeting is by using folic acid. Vitamin B9 or pteroylglutammate, commonly known as folate, is a non-immunogenic hydrosoluble vitamin important in the DNA and RNA synthesis and repair, as well as, protein and haemoglobin formation. [16] Folic Acid (Fig 1.3) is a inexpensive synthetic vitamin, stable over a broad range of temperatures and pH values. It is non-immunogenic and can bind to the folate receptor even if modified. It can be modified to connect to a particle or marker, and it's incorporated via receptor-mediated endocytose to the interior of the cell. The internalization occurs directly by membrane invagination. When the pH inside the vesicle reaches 5 (acidic medium), the folic acid disassociates from the receptor, releasing the combined particles to the cytosol while the folate-receptor returns to the membrane. Some cancers (epithelial, ovarian, cervical, breast, lung, kidney, colorectal, and brain tumours) have the folate receptor over-expressed, due to the high rate of cellular proliferation that requires nucleotide bases to replicate their DNA when compared to normal tissue. Nevertheless, this is not expected in sarcomas, lymphomas, pancreatic, testicles, bladder, prostate, and liver cancers. [16] Therefore, the high-affinity receptors can be exploited as an active target for some cancer treatment and non-invasive detection. The folate that is not captured by the receptors is expelled from the body, mostly by the kidneys. [16, 18]

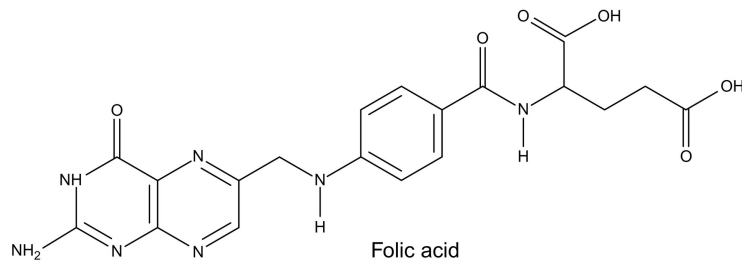


Figure 1.3: Structure of Folic Acid. [19]

## 2 Nanoparticles

Nanotechnologies are considered to have been introduced by physics Nobel laureate Richard P Feynman in 1959, but the term was invented by Norio Taniguchi, a professor from Tokyo University of Science, in 1974. [20] It is an interdisciplinary area of study, manipulation and control of materials at the nano scale. Several elements can be combined to develop different properties, with common nanoscale materials. They frequently manifest different features from the bulk material, such as superparamagnetic behaviour or higher chemical reactivity and electrical conductivity, due to quantum and surface boundary effects. [20]

Nanoparticles (NP) are characterized by having diameters under 100 nm, being the more stable form is spherical. This high surface to volume ratio allows the particle to carry large molecular payloads. The surface can be modified physically or chemically for example, by adding targeting groups or redefining the surface charge to better fit the pretended goal. The composition is defined based on the objective, and can be classified into organic (e.g. liposomal formulations for Kaposi's sarcoma and ovarian cancer), inorganic (e.g. iron oxide nanoparticles for glioblastoma therapy and as contrast enhancers for magnetic resonance imaging) or hybrid. (Fig.1.4). [18, 21]

Nanoparticles have gained interest for theranostic (therapeutic and diagnostic) systems. One group with great results in biomedical applications are Silica Nanoparticles (SiNPs), which have been used as carriers and supports in catalysis, drug delivery, imaging, etc. The advantages of SiNPs include the facility to control their diameter with low size dispersion, biocompatibility and lower aggregation compared to polymer-based nanoparticles. [16, 21]

One way to produce SiNPs is by the Stöber method, a sol-gel method, developed in 1968 by Werner Stöber, Arthur Fink and Ernst Bohn. [22] This process involves a colloidal solution to get well-defined particles with uniform composition. The morphology of the particles can be easily tuned, by simply adjusting reaction parameters, and can be used in multiple applications such as ceramics, chromatography, catalysis, paints, pharmaceutical, optical imaging, etc. [23]

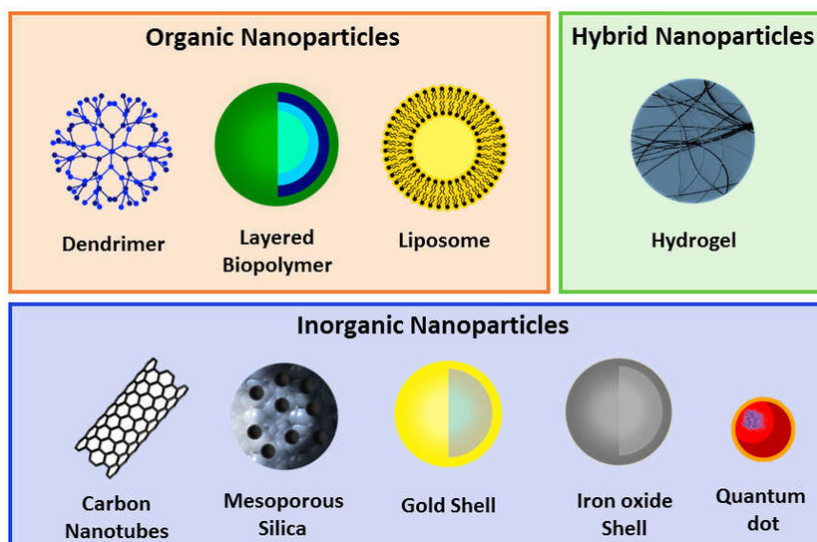


Figure 1.4: Schematic representation of different types of nanoparticles (NPs) divided into organic, hybrid and inorganic categories. [24]

The sol-gel reaction can use ammonia as catalyst, to hydrolyze the silica precursor, followed by condensation. The hydrolysis process is shown below, in fig 1.5. Using TEOS as silica precursor, in a base-catalysed reaction, the hydrolysis of TEOS by  $\text{OH}^-$  ions initiates a nucleophilic substitution of an ethoxy group (Si-OR) by silanol groups (-Si-OH). This exchange increases the positive charge of silicon and reduces steric hindrance, improving the rate of conversion. [23]

In fig 1.6, the condensation phase, silanol groups (-Si-OH) condense to form siloxane bonds (Si-O-Si), with the release of water. [23]

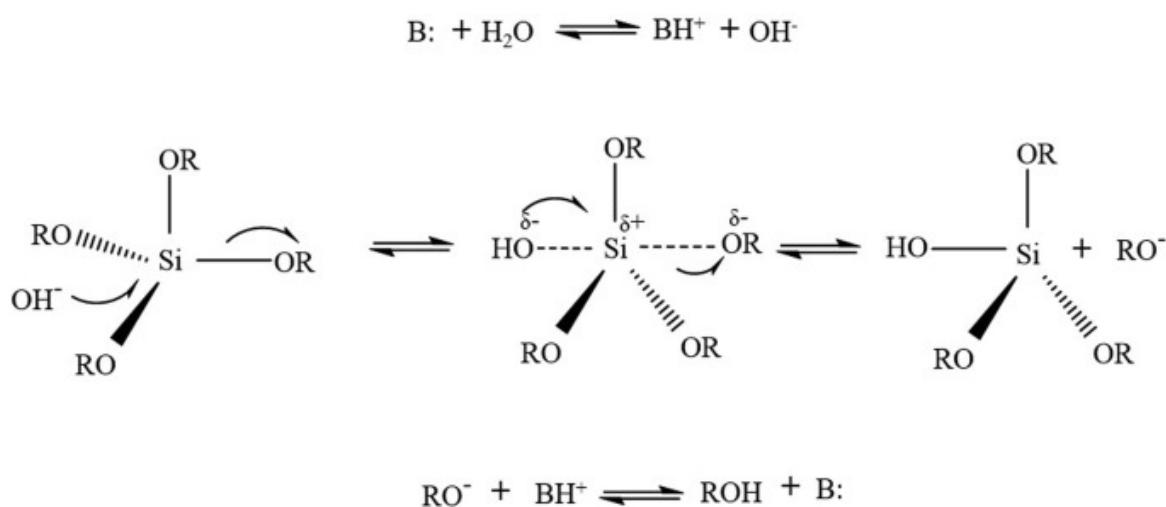


Figure 1.5: Mechanism of hydrolysis of TEOS precursors in base (B:)-catalyzed reactions. [23]

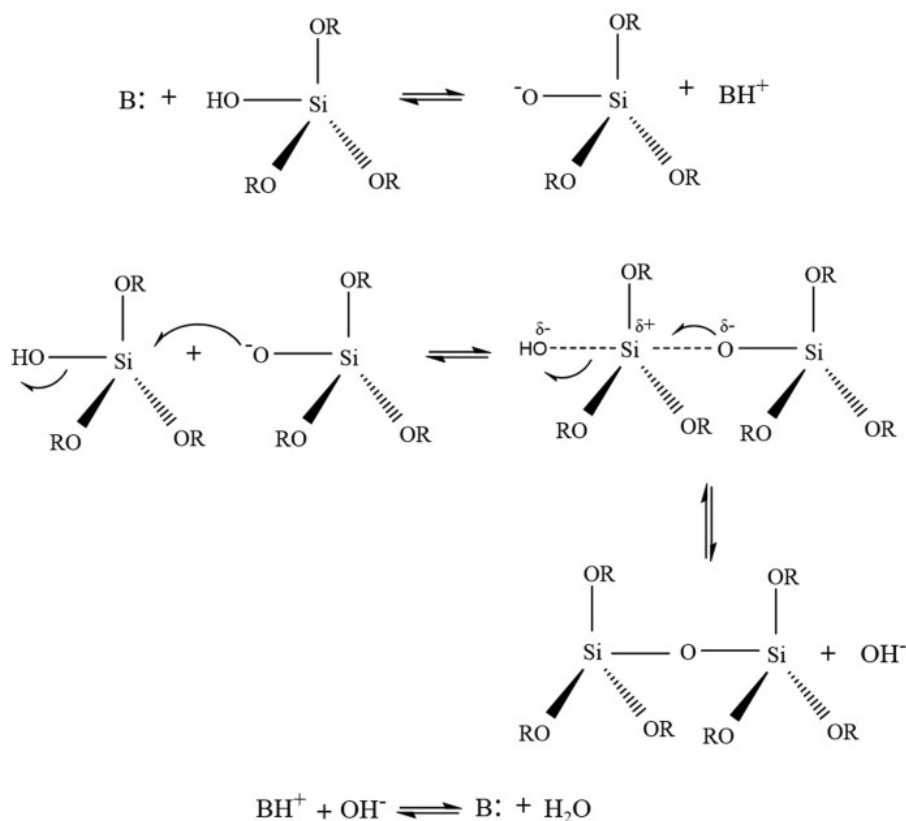


Figure 1.6: Mechanism of condensation of TEOS precursors in base (B:)-catalyzed reactions. [23]

Some of the parameters that influence the diameter of the NP are the temperature, the silica precursor, the solvent and the pH. First, the absence of ammonia as a catalyst leads to silica flocculation and irregular shaped particles. After its addition, the increased concentration leads to larger spherical particles with a decrease in polydispersity. The rest of the factors have influence mostly on the hydrolysis rate, that will consequently define the particle size obtained and its polydispersity. [22, 23]

As the temperature increases, the rate of hydrolysis also increases, facilitating particle nucleation and thus leading to smaller particles. Contrarily, at lower temperatures the rates of hydrolysis and nucleation decrease leading to larger particles. [10] Silica sources with large carbon chains are more easy to control and have slower hydrolysis resulting in larger NPs. [22, 23] Different solvents also have different polarity. The size of the carbon chain will influence the dielectric constant. Longer primary chains have a smaller dielectric constant values and consequently bigger particles. [23] At pH=2, we have the isoelectric point of silica and the hydrolysis rate constant is extremely low. So at pH<2, we have a reaction under acid catalysis. The reaction is usually performed under basic conditions to ensure the negative charges on the surface of the particle and minimize aggregation. [22, 23]

During the synthesis, the incorporation of dye into the matrix is possible. This ensures the loading of multiple dye molecules in a single NP, so we can expect an elevated brightness and higher signal to background ratio. When inside a particle, the diffusivity of oxygen is lower, creating a protective environment from oxidative degradation of the dye, ensuring photostability. [25] Better photostability ensures more constant fluorescence during surgery, and minimal effects on the immune system from production of toxic photo-degradation products. [9, 25]

### 3 Objectives

During excision of a tumour, the removal of all cancerous cells is extremely important to minimize the recurrence rates. To help surgeons, fluorescent probes are used to better define the tumour margins. The objective of this thesis is to develop tumour targeting fluorescence nanoparticles for fluorescence guided surgery.

In general, when a dye is applied to the body via traditional methods (oral, intravenous, subcutaneous) it can suffer modifications and especially degradation due to pH or protein binding. As its dispersed through the entire body, also limits its availability and increases the unwanted effects in other organs. [15] Our goal is to develop a nanoparticle with an incorporated dye, that can both protect the dye and ensure its accumulation on tumour tissues. We choose Silica Nanoparticles (SiNPs), since they are biocompatible, easily internalized by the cell and have a straightforward production.

For developing the system, an easy to produce perylenediimide dye derivative was used. Perylenediimides are dyes with a good photochemical and thermal stability, photophysical properties that can be tuned, replacing substituents, in the perylene core positions (structure represented in fig 1.7). It is a strong electron acceptor and has a large fluorescence quantum yield making PDI a multiple application material, with studies in the health industry in addition to electronics and solar systems (for example, organic solar cells). The initially incorporated dye into the Silica Nanoparticles was the bis(propyl)triethoxysilane perylenediimide, usually known as pigment red 179 (Fig. 1.7). [7] However, it is not an approved fluorescent probe for FGS.

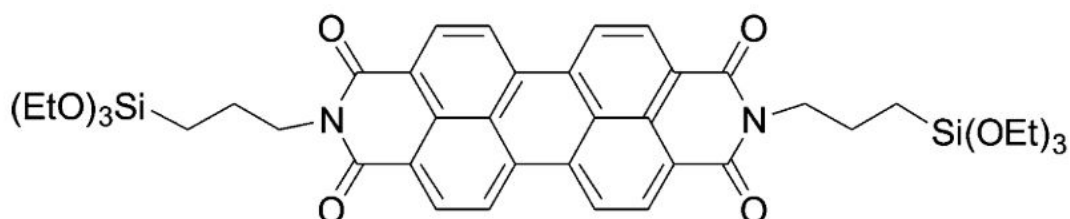


Figure 1.7: Structure of bis(propyl)triethoxysilane perylenediimide. [26]

To improve tumour affinity, we used folic acid as an active targeting agent. Since our goal was to functionalize only the external layer, without compromising the structure and size dispersion, the functionalization process chosen was post-grafting, with the carboxylic acid of the folate reacting with the amine-functionalized SiNP. [27, 28] In the two steps route, the particles are activated with APTES, washed and then the folic acid is added to the SiNPs and in the one, a mixture of APTES and Folic Acid is left stirring and then the particles are added.

After testing and characterizing the synthesis and both functionalization processes with PDI, we began using the chosen FGS dye, FIGS-IST-Dye1 (Fig. 1.8). This compound is an altered form from the IRDye800CW family. Its emission is in the NIR (outside the range of biological auto-fluorescence), allowing a good differentiation of tumour and healthy tissue. The alkoxide groups present on its structure allows its incorporation inside the silica network during the Stöber process, by a covalent bond with the reactive organosilicates. [10]



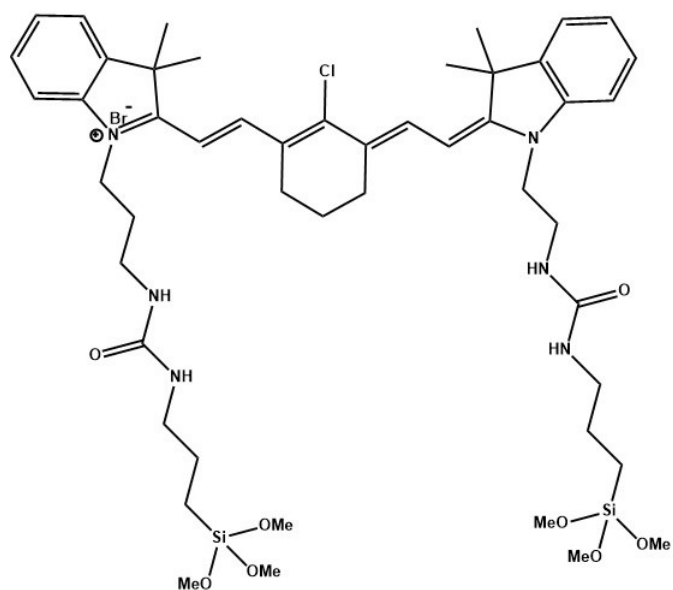


Figure 1.8: Structure of FIGS-IST-Dye1.

The dye containing SiNPs is biocompatible but, since our goal is to use it in Fluorescence Guided Surgery (FGS), we need to reassure that there is no toxicity. So we performed a cell viability test to assess the biocompatibility of the final system.



## Chapter 2

# Experimental Procedure

### 1 Reagents and Solvents

Ammonium hydroxide solution ( $\text{NH}_4\text{OH}$  basis, 28.0–30.0%), Tetraethyl orthosilicate (*TEOS*,  $\geq 99.0\%$ ), 3-aminopropyl triethoxysilane (APTES, 99%), N,N'-Dicyclohexylcarbodiimide (DCC, 99%), Dimethyl Sulfoxide (DMSO, anhydrous,  $\geq 99.9\%$ ) were purchased from Sigma-Aldrich. Ethanol ( $\geq 99.8\%$ ), N,N-Dimethylformamide (DMF, HPLC grade,  $\geq 99.9\%$ ) and s-Trioxane (1,3,5-trioxane, 99+%) from Honeywell Fluka, Fisher Scientific. Dichloromethane (DCM, HPLC- Isocratic grade- Stabilized with amylene) from Carlo Erba. Molecular sieves (3A, 2-5 mm, Hygroscopic) from Alfa Aesar. PrestoBlue™ (PB) used from Invitrogen by ThermoFisher Scientific, Carlsbad, CA, USA. Dulbecco's Modified Eagle's Medium (DMEM) and Fetal Bovine Serum (FBS) from gibco and penicillin-streptomycin all bought from Thermo Fisher Scientific. L929 cell line purchased from European Collection of Authenticated Cell Cultures.

Argon (Ar) ( $\geq 99.9999\%$ ) used from Alphasgaz, Air Liquide. Perylenediimide (PDI) was synthesized according to literature procedures [26]. Deionized water from a Millipore Milli-Q system was used for the preparation of dispersions.

### 2 Equipment

#### 2.1 Centrifuge

Avanti J-30I centrifuge with a rotor JA-30.50 was used with 50 mL Centrifuge tubes both from Beckman Coulter for all the centrifugations carried in the study.

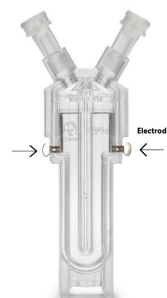
#### 2.2 Dynamic Light Scattering (DLS)

Zetasizer Nano-ZS, with a 532 nm laser, was used to measure the hydrodynamic particle diameter ( $D_h$ ) via Dynamic Light Scattering. The measurements were obtained using a disposable polystyrene cuvette (fig.2.1a). The autocorrelation functions were analysed by the general purposes analysis mode, available in the Zetasizer Software. To prepare for measurements, a single droplet of a 3.3 mL single use pipette is mixed with 1 mL of Milli-Q water, if the particles were dispersed in the initial solution. If the particles are dried, 1 mg of SiNPs was dispersed in 1 mL of Milli-Q water. In DLS it is also possible to measure the zeta potential of the dispersion. This value indicates the degree of electrostatic repulsion between charged particles in the suspension. Higher absolute values suggest good stability while smaller ones point out attractive forces exceeding the repulsion, leading to aggregation. To measure the

Zeta Potential, 1 mg of particles is dispersed in 1 mL of Milli-Q water, ultrasonicated to ensure dispersion and transferred to a Zeta cell (fig.2.1b).



(a) Disposable DLS Cell.



(b) Zeta Potential Cell.

## 2.3 Fluorescence Spectroscopy

Steady-state and time-resolved fluorescence spectra were obtained using a Horiba Jobin Yvon Fluorolog 3-22 spectrofluorometer (Kyoto, Japan) with a 450 W xenon lamp, with double-grating monochromators in excitation (laser dye DCM, 610–680 nm, 130 mW, 5 ps, 4 MHz) and emission (collected at the magic angle using a Jobin Yvon iHR320 monochromator (Horiba Jovin Ivon Inc.). For the spectra measurements approximately 2 mg of SiNP-PDI were used and 1 mg of SiNP-FIGS-IST-Dye1 dispersed in 1 mL of solvent, ultra-sonicated and transferred to a 5 mm path length quartz cuvette.

## 2.4 Nuclear Magnetic Resonance (NMR)

$^1\text{H NMR}$  spectra were obtained by a Bruker 300 MHz spectrometer (Bruker BioSpin GmbH, Rheinstetten, Germany). To prepare the samples, approximately 8 mg of SiNPs were dispersed in 400  $\mu\text{L}$  of  $\text{NaOH} + \text{D}_2\text{O}$  and 50  $\mu\text{L}$  of Trioxane (internal reference with known concentration), the mixture was ultrasonicated for 1h and transferred to a 5 mm NMR sample tube.

## 2.5 Transmission Electron Microscopy (TEM)

TEM images were obtained using a Hitachi, model H-8100, equipped with an accelerator with maximum voltage of 200 kV and a LaB6 filament. The TEM is equipped with a KeenView camera (Soft Imaging System) for digital image acquisition. The images obtained were processed using ImageJ software. The samples preparation method used was dehydration, starting by dispersing the particles in ethanol and dipping the copper grid coated with carbon onto the solution. They are then left to air dry.

## 2.6 UV/Vis Spectroscopy

Jasco V-660 UV-VIS Spectrophotometer (Oklahoma City, OK, USA), with a double monochromator and photomultiplier tube detector, was used for linear absorption spectrum measurements. The cells were prepared following the procedure described for Fluorescence Spectroscopy.

## 2.7 Microplate Reader

POLARstar Optima Multidetector Microplate Reader with Fluorescence Polarization (BMG LABTECH, Germany) was used in the fluorescence intensity mode.

### 3 Synthesis of Stöber Silica Nanoparticles

The dye in use, PDI and then FIGS-Dye-IST1, (5 to 10 mg) was dissolved in a small quantity of absolute ethanol and ultra-sonicated. The solution was filtered through a 0.2  $\mu\text{m}$  cellulose filter, to remove insoluble clusters, and transferred into a 250 mL polypropylene flask. Ethanol, Mili-Q Water and  $\text{NH}_4\text{OH}$  were added (Table 2.1) after, TEOS was added to the mixture and the temperature was increased to 40 °C, and left overnight. The nanoparticles were centrifuged and washed three times with absolute ethanol (90 000G, 20 min). The particles were dried in an oven at 60 °C overnight. The amount of NP collected was around 500 mg in each synthesis.

Table 2.1: Reagents quantities used in the different synthesis.

Synthesis	Absolute Ethanol (g)	Mili-Q $\text{H}_2\text{O}$ (g)	$\text{NH}_4\text{OH}$ (mL)	TEOS (mL)
Si1	86.656	9.021	1.51	4.46
Si2	64.656	9.021	1.51	4.46
Si3@PDI	86.656	9.928	1.51	4.46
Si4@PDI	86.656	9.526	1.51	4.46
Si5@FIGS	86.656	9.928	1.51	4.46
Si6	866.56	90.21	15.1	44.6

The one litre reaction was performed, without any dye, to evaluate the possibility of scaling up the process. All the reagents quantities were multiplied by 10 times. 50 mL from the initial solution (Si6A) were transferred to a 250 mL PP flask (Si6B) for direct comparison. After drying, 11 g were collected from the reaction Si6A.

### 4 Surface functionalization of Silica Nanoparticles

To functionalize the SiNPs, two different routes, one and two steps routes, were followed in order to determine the more reproducible one. The quantities of APTES used was tailored to each experiment, to deliver two molecules per  $\text{nm}^2$ .

#### 4.1 Two Steps Route

The following procedure was performed as described in [27], and we can see the schematic representation in fig.2.2. Initially, SiNP(0.250 g) were added to 4.5 g of toluene, and ultrasonicated. APTES (0.0191 g) was added and the reaction was left stirring at 120 °C for 48 h. The SiNP were collected and washed with absolute ethanol three times (90 000 G, 20 min).

The second steps starts by degassing with argon in a 50 mL round bottom flask, FA (0.0148 g) and DCC (0.1370 g). After, dry DMF (3 mL), DMSO (1 mL) and the amino functionalized particles dispersed in DMF were added and the mixture was left stirring overnight at room temperature. The particles were washed with DCM and absolute ethanol three times (90 000 G, 20 min).

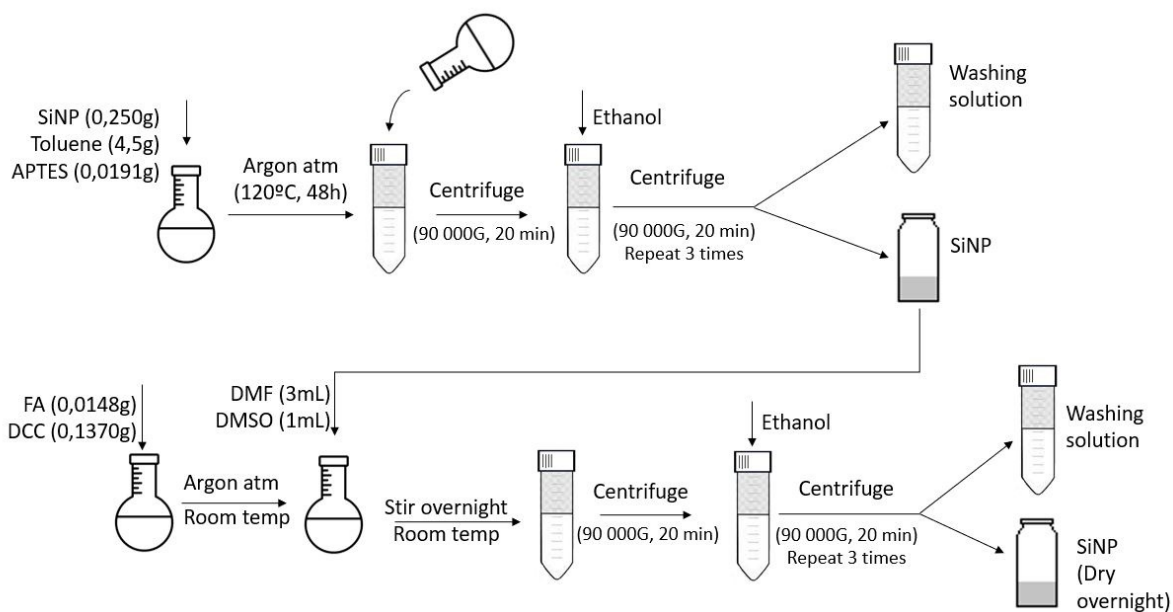


Figure 2.2: Schematic representation of functionalization of a SiNP with folic acid via two steps route.

## 4.2 One step Route

The following procedure was performed as described in [28], and we can see the schematic representation in fig.2.3. DMSO (2.0509 g), FA (0.0607 g), DCC (0.0327 g) and APTES (0.0387 g) were mixed in a 50 mL round bottom flask and left stirring, under argon atmosphere, for 6 h at room temperature. After, 126 mg of SiNP were dispersed in 12 mL of toluene and added to the reaction mixture. The reaction was left stirring for 72 h, at room temperature. Thereafter, the NPs were washed three times with absolute ethanol and dried in the oven.

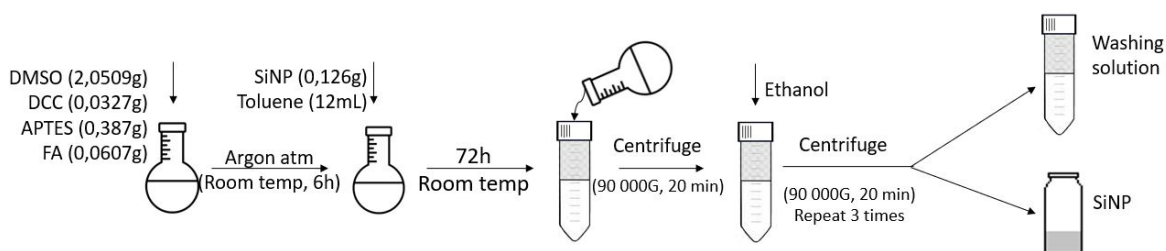


Figure 2.3: Schematic representation of functionalization of a SiNP with folic acid via one steps route.

## 5 Cell Viability

The toxicity effect of the NP was evaluated by resazurin based assay using PrestoBlue™ reagent. Briefly, L929 murine fibroblast cell line were seeded in 96-well tissue cultured plates at initial density of  $1 \times 10^4$  cells per well and left overnight in CO<sub>2</sub> incubator (5%) at 37 °C. Then, cell medium (DMEM supplemented with 10% FBS and 1% penicillin-streptomycin) was discarded and replaced with a solution of different NP doses previously prepared in complete cell culture medium. L929 cells were incubated for additional 24 h. Finally, the PB viability assay was performed accordingly with PrestoBlue™ reagent kit protocol. The resazurin conversion into resorufin was monitored by measuring fluorescence intensity (excitation 530 nm, emission 590 nm) in a microplate reader (BMG Labtech, Polar Star Optima) at 37 °C. The test were performed by Adriana Bastos Cruz.





# Chapter 3

## Results and Discussion

### 1 Synthesis of Silica Nanoparticles

As previously described, the SiNP were synthesized using the Stöber method. Initially, two syntheses (Si1 and Si2) were performed without any modification just to learn the process. In the next particle synthesis, a dye was incorporated into the reaction mixture. In reactions 3 and 4 we incorporated PDI, and in reaction 5 FIGS-IST-Dye1. The quantities were presented in table 2.1.

After each synthesis, the particles diameters were measured using Dynamic Light Scattering (DLS) and TEM. The diameters were obtained at room temperature and the results are shown in Table 3.1. DLS values by number, were obtained from the average of 5 measurements and the TEM diameters were obtained from 70 particles, using image software ImageJ.

Table 3.1: Diameter of the SiNP measured by DLS and TEM.

Particles	DLS	TEM
	Average diameter (nm)	Average diameter (nm)
Si1	40 ± 3	39 ± 3
Si2	80 ± 3	80 ± 3
Si3@PDI	24 ± 1	24 ± 3
Si4@PDI	32 ± 1	32 ± 3
Si5@FIGS	37 ± 2	33 ± 3
Si6A	65 ± 2	65 ± 5
Si6B	66 ± 3	69 ± 7

TEM measurements are similar with the number average diameter obtained by DLS. Since DLS measures the hydrodynamic diameter it is common to have values slightly bigger due to the solvent ions interacting with the nanoparticles. [29]

While comparing both tables 2.1 and 3.1, we can confirm that increasing the water quantities, consequently smaller concentrations of ammonium hydroxide and lower pH, leads to smaller particles due to a decreased rate in the condensation phase. [10] From the correlograms (fig. 3.1 and appendix A)) and the diameters standard deviation (the higher value is 12,5 %), we can confirm that all the particles were fully dispersed and with uniform sizes. If aggregates were present, the lines would not converge to zero. [30]

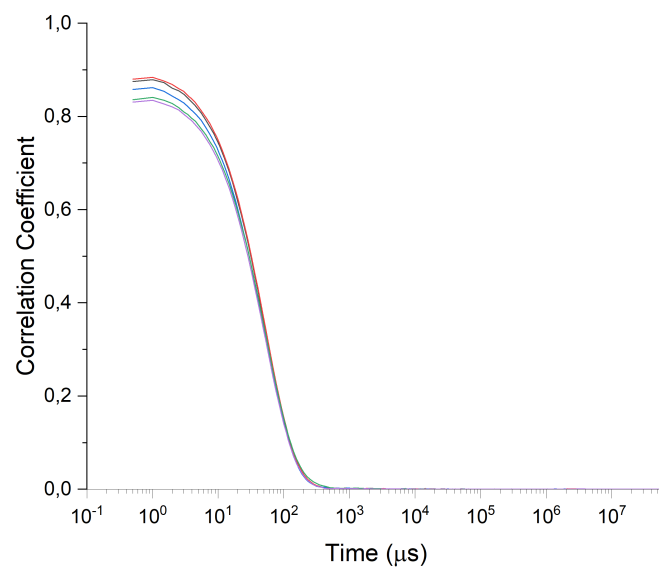


Figure 3.1: Correlograms obtained by DLS for Si3@PDI.

TEM imaging allows direct visualization of the particles and ensure their morphology and dimensions are under the target values (the optimal range for particle uptake is 30-50 nm). In fig.3.2, SiNP reveal spherical morphology and uniform size distribution (Table. 3.1). Some aggregation is present that can be justified by sample preparation protocol.

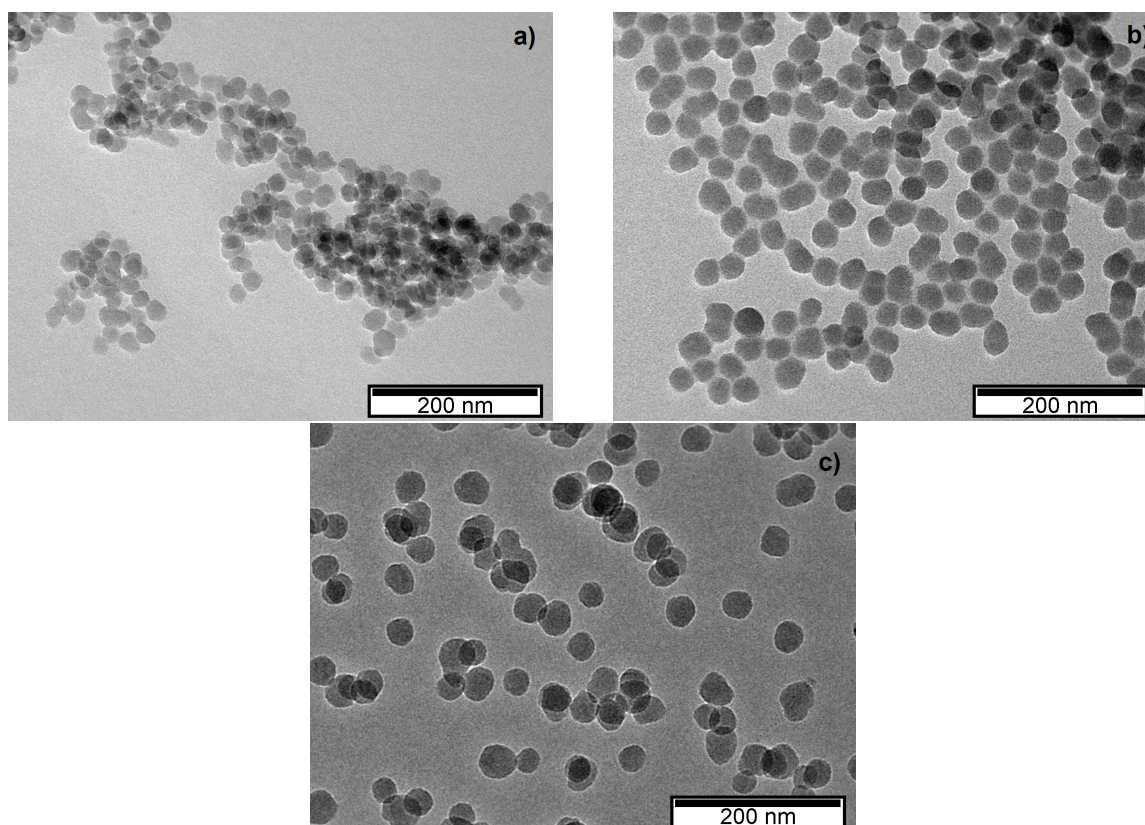


Figure 3.2: TEM images from reactions: Si3@PDI (a), Si4@PDI (b), Si5@FIGS (c).

Nonetheless, after centrifuging Si5@FIGS, a pink solution was obtained, instead of the normal transparent or greenish like the dye. This colour was a result of the reactional solution. After the first centrifugation, all the other washes solution were transparent. From the TEM images, no structural differences appears to be present, so more tests need to be performed to clarify the cause of such colour.

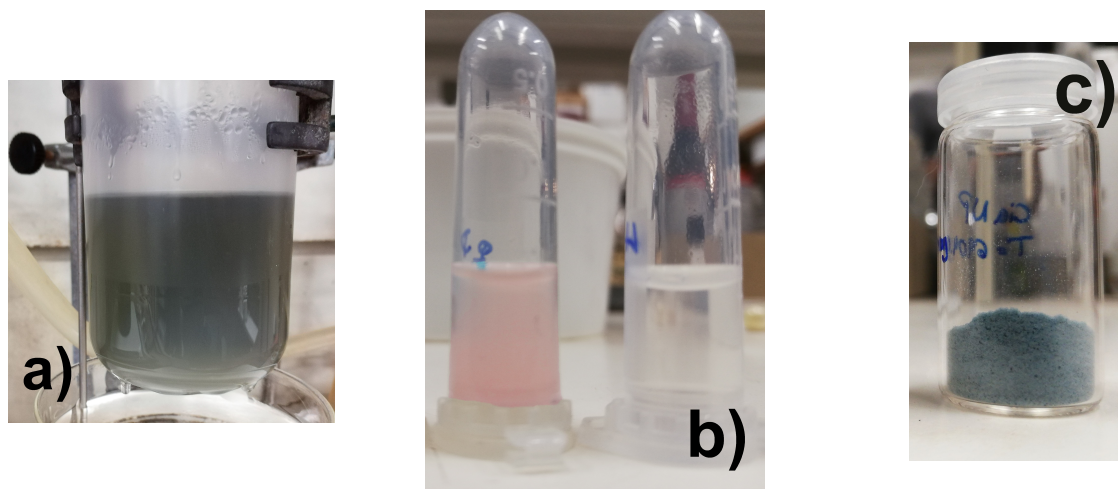


Figure 3.3: Reactional mixture of Si5@FIGS synthesis, before centrifugation (a); supernatant obtained in the first wash (b, left) and second wash (b, right); particles Si5@FIGS after washed and dried (c).

In fig. 3.4, we can see the particles synthesized in large quantities (Si6A). Some solution was transferred to a smaller flask (Si6B) giving us room for comparison. We can confirm that both solutions reached a spherical and uniform morphology, having the smaller solution (Si6B) resulting in slightly bigger particles. The quantities used for this reaction were the same used in the first test synthesis (Si1). Si1 was performed at 40 °C while Si6A and B were at room temperature, explaining the higher diameter values for Si6. Higher temperatures lead to higher hydrolysis rates and therefore an outburst of nucleation points that creates smaller particles. [23]

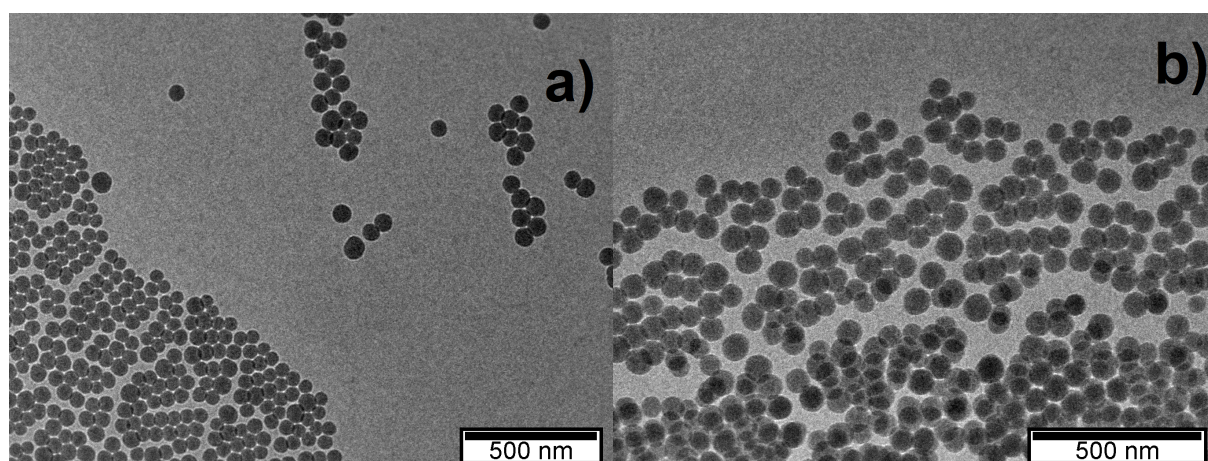


Figure 3.4: TEM images from reaction: Si6A (a), Si6B (b).

## 2 Silica NP Functionalization

To promote the selective targeting of cancer cells, the particles were externally modified with Folic Acid (FA). First, the particles were functionalized with 3-aminopropyl triethoxysilane (APTES) to replace the hydroxyl group for an amine. This amine will attack the carboxylic group of the folic acid, and replace it.

To evaluate the incorporation, two procedures were tested. A two steps route schematic representation in fig.2.2, were the particles are activated with APTES, washed and only then the folic acid is added to the SiNPs. In the one step route, schematic representation in fig. 2.3, were the mixture of APTES and Folic Acid is left stirring and then the particles are added.

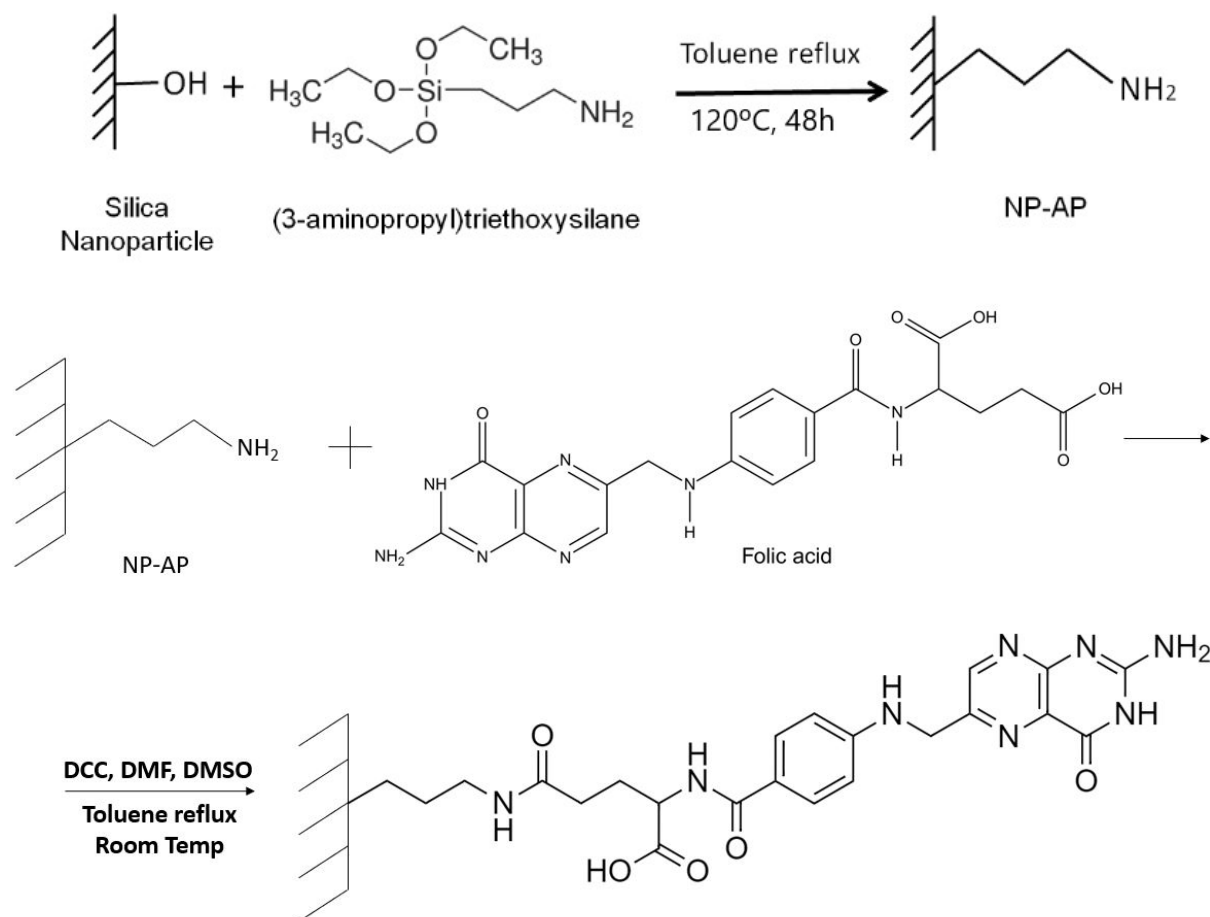


Figure 3.5: Schematic representation of functionalization of a SiNP with folic acid via two steps route.

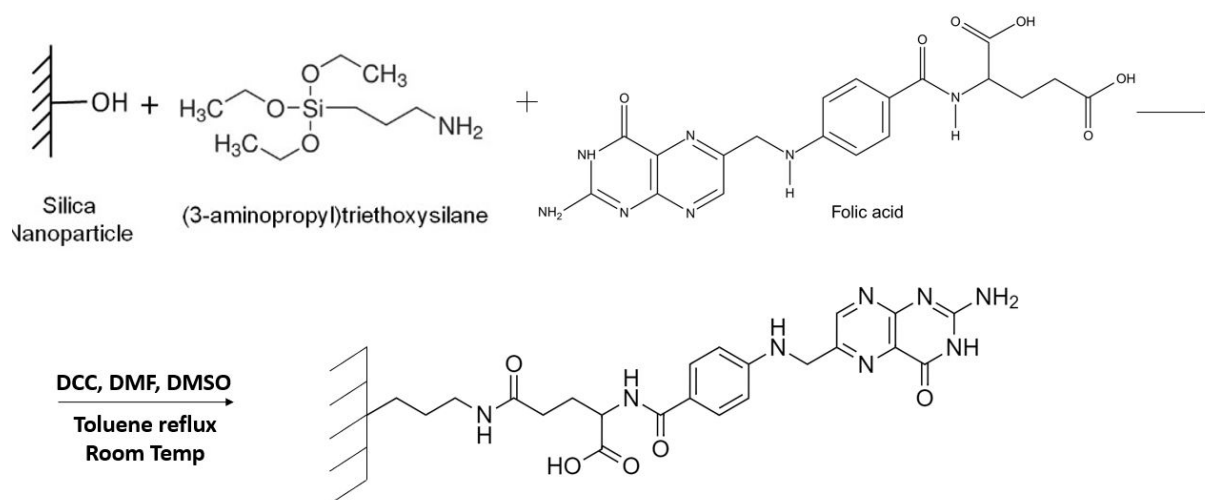


Figure 3.6: Schematic representation of functionalization of a SiNP with folic acid via one steps route.

The carboxylic group present in the folic acid (fig. 1.3), is driven by *N,N'*-Dicyclohexylcarbodiimide, attacked and suffers a nucleophilic substitution by the amine left from the APTES functionalization connecting to the SiNP. [31] The particles obtained after drying are shown in fig. 3.7.

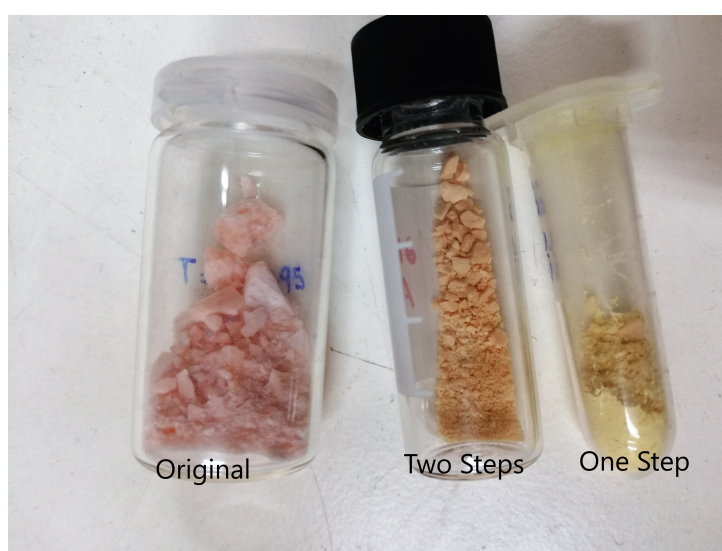


Figure 3.7: Si3@PDI from left to right: before functionalization, functionalized by the two step procedure, functionalized by the one step procedure.

After functionalization, the Zeta potentials were measured to confirm the modification. When functionalizing there is a substitution of the alcohol groups by amines. Since alcohols are more negatively charged, when replacing them we can see an increase in the zeta potential value. The results are presented in Table 3.2.

Table 3.2: Zeta Potential in multiple functionalizations.

Reaction	Original (mV)	Two Steps (mV)	One Step (mV)
Si3@PDI	$-36.1 \pm 0.4$	$-24.9 \pm 0.5$	$-1.4 \pm 0.3$
Si5@FIGS	$-27.2 \pm 0.1$	$-3.1 \pm 0.7$	-

The one step functionalization process was not reproduced in the Si5@FIGS nanoparticles for lack of reliability as we will explain further ahead. Values closer to 0 tend to lead to flocculation of the particles.

To quantify the amount of folic acid incorporated, we used Nuclear Magnetic Resonance (NMR). A strong base is added with an internal standard, both in a deuterated solvent. The base (NaOH), dissolves the silica network and releases the surface-bound groups into the solution, and the reference used was trioxane.

For comparison, a spectrum of non functionalized particles was obtained (Fig 3.8). We can identify at 4.79 ppm the D<sub>2</sub>O peak that works as a reference to correct spectrum shifts. At 5.18 ppm we have trioxane and, at 3.55 and 1.07 ppm we observe the ethoxy groups (respectively from the CH<sub>2</sub> and CH<sub>3</sub>), corresponding to residual ethanol from washing the particles, that remains entrapped in the matrix even after drying. [32]

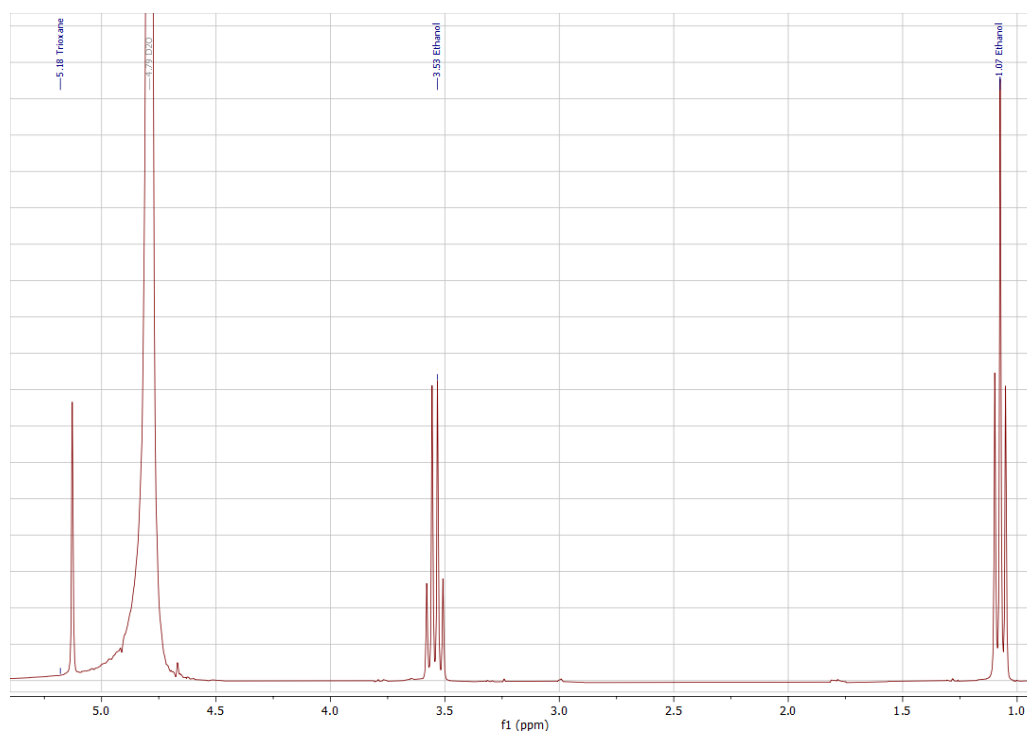


Figure 3.8: <sup>1</sup>H NMR of non functionalized Si3.

This method allows the quantification of each functional group added to the SiNPs, due to the presence of trioxane. The reference is added in a known concentration so that we can use its peak to extrapolate the concentration of the other molecules. In figure 3.9, the spectrum of Si3 functionalized by the 2-step method, shows the peak assignment for the carbon chain and amine left from APTES, and for the folic acid. The other spectra are presented in appendix. In Table 3.3, we show the results obtained from peak integration.

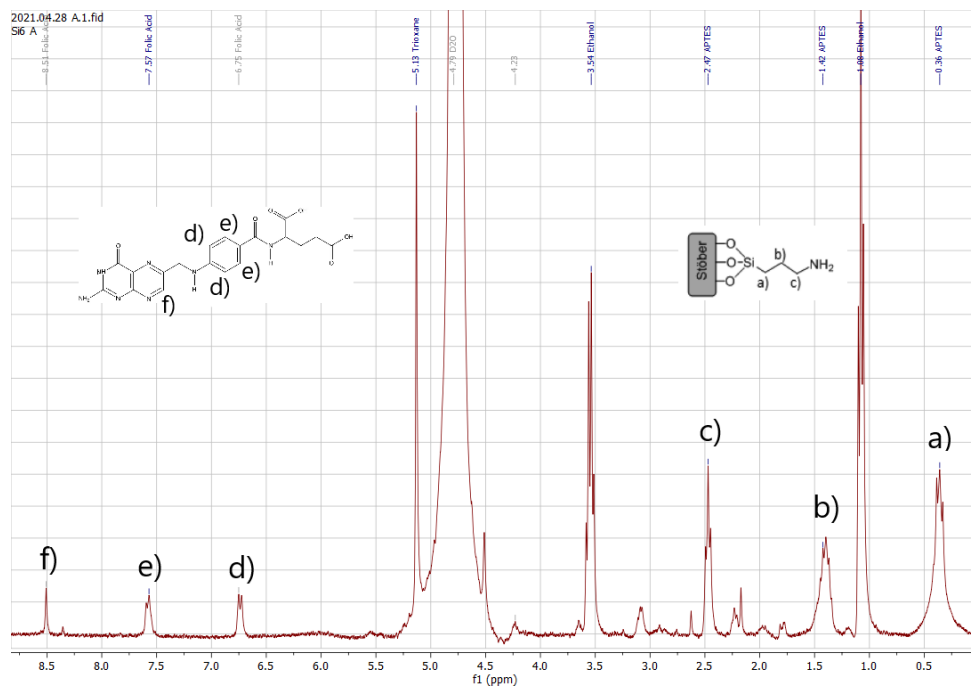


Figure 3.9: <sup>1</sup>H NMR of Si<sub>3</sub>-PDI functionalized by the Two Step method, with peaks assignment.

Table 3.3: Quantification of SiNPs functional groups (mM of APTES/Folic acid by gram of SiNP, molecules per nm<sup>2</sup> of SiNP surface and molecules per SiNP.

Reaction		mMol/g	molecules/nm <sup>2</sup>	molecules/particle
Two Step (Si3)	APTES	0.41	1.56	2830
	Folic Acid	0.15	0.59	1067
One Step (Si3)	APTES	2.9	11.26	20379
	Folic Acid	0.77	2.99	5420
One Step (Si4)	APTES	2.18	11.19	35992
	Folic Acid	1.32	6.80	21872
Two Step (Si5)	APTES	0.55	2.89	9902
	Folic Acid	0.12	0.64	2182

When functionalizing the SiNPs, the amount of APTES used was calculated to have a surface coverage of 2 molecules/nm<sup>2</sup>, to ensure a good functionalization without overlapping of APTES. Some variations are expected, so the values obtained by the two steps method are reliable. The smaller quantities of Folic Acid when compared with APTES are explained by the larger size of the folic acid molecule (occupies more volume). When we look at the values obtained in Si<sub>3</sub> by the one step procedure, we can presume to be wrong because it is not physically possible. The same procedure was repeated for Si<sub>4</sub>, to ensure if it was not an experimental error, and once again the values are not physically acceptable. This high values can be a result of folic acid and APTES condensation, leaving aggregates. Therefore, the system with FIGS-IST-Dye1, only the two steps method was used results.

### 3 Fluorescence Studies

The main goal of the work is to allow a better identification of tumour tissue during fluorescence guided surgery. So we have to ensure that the fluorescence properties of the dyes are preserved during

synthesis.

The fluorescence spectrum of PDI, in toluene without any modifications has peaks at 537, 559 and 628 nm [33]. After incorporating in the silica matrix and functionalization, we obtained the spectrum in fig.3.10. As we can see, the spectrum of PDI in the particles is similar to that of the free dye. The integrity of the dye was not compromised by incorporation into the SiNP and the presence of the folate groups does not interfere with the fluorescence. The spectrum presents a mirror image and a small Stokes shift between emission and excitation. Absorption spectra were also obtained but, due to light scattering of the silica nanoparticles, no peaks were visible.

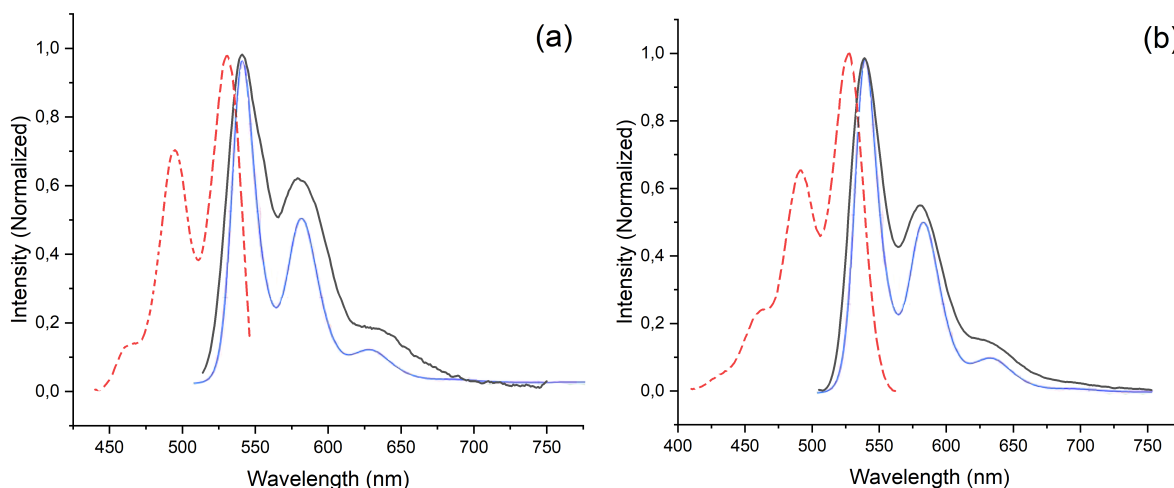


Figure 3.10: Normalized fluorescence spectrum of (a) Si3@PDI, functionalized via One Step method in H<sub>2</sub>O and (b) Si4@PDI functionalized via Two Step method in H<sub>2</sub>O. In dashed red, we have excitation curves (em= 580 nm) and at solid black, emission curves (ex=490 nm). In blue we have the spectrum of PDI before synthesis, in toluene.

The same study was performed for the Si5@FIGS particles (Fig.3.11 and 3.12). When incorporated into the nanoparticle, there are no visible peaks due to the SiNPs scattering.

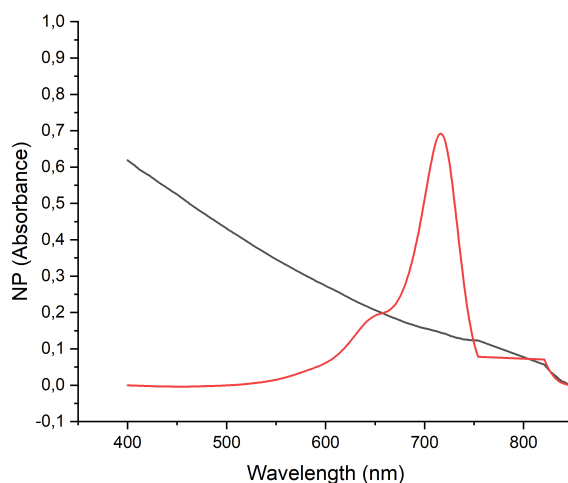


Figure 3.11: Absorption spectrum of free FIGS (red) in methanol, and Si5@FIGS (black).



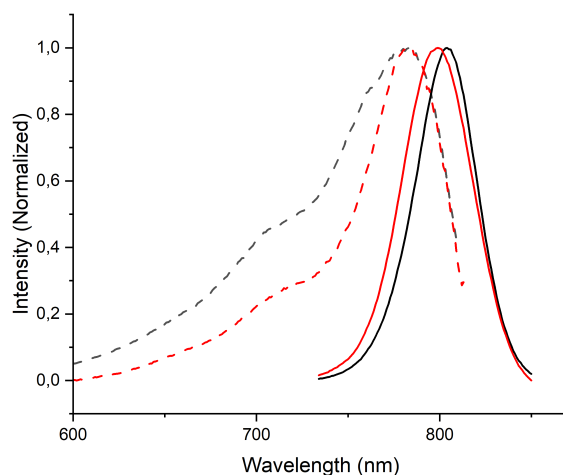


Figure 3.12: Normalized fluorescence spectrum of Si5@FIGS (red) in H<sub>2</sub>O and free FIGS-IST-Dye1 (black) in methanol. Excitation (dashed curves) of the NP measured at 840 nm, and of the free dye at 825 nm. Emission (solid curve) of the NP measured at 680 nm, and of the free dye at 710 nm.

The spectrum presents a shift from the free dye to the particle caused by the use of different solvents in each measurement (methanol for FIGS, water for the SiNPs). In this range we can see that there were no changes in the fluorescence of the dye, when incorporated in the SiNPs. But if the excitation is further away from the main peak (790 nm) we can see a new peak, at 613 nm, that was not expected (fig.3.13). That new peak can be associated with the presence of colour in the reaction mixture after centrifuging (fig.3.3 (b)). A spectrum of the reaction mixture was taken (fig.3.14), showing that the component left has the same emission wavelength has the new peak at Si5@FIGS. A possible explanation is that some of the dye was degraded due to the synthesis pH. One advantage of the unexpected degradation is that now the SiNPs are fluorescent in visible light.

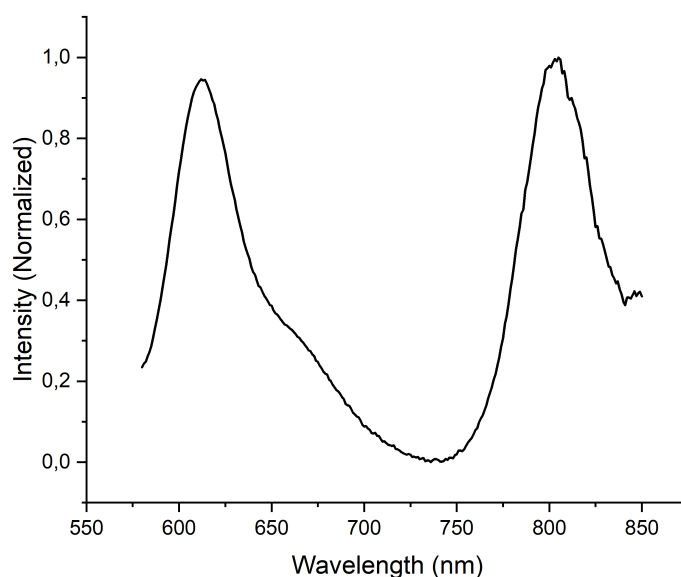


Figure 3.13: Emission spectrum of Si5@FIGS with excitation at 550nm.

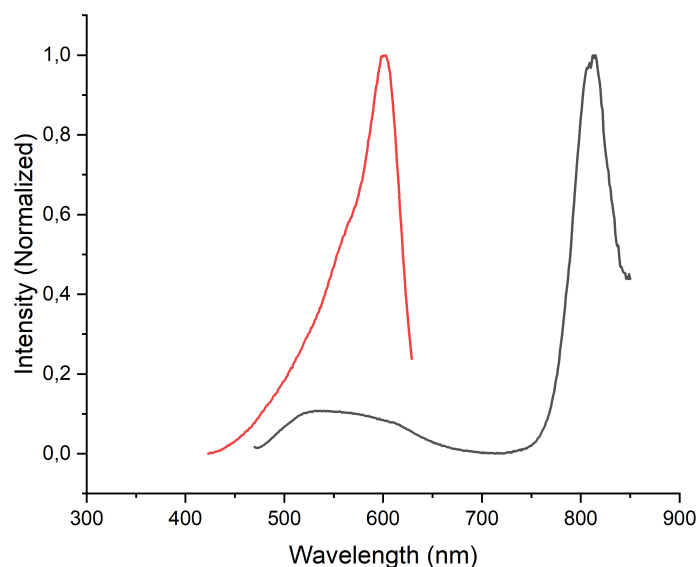


Figure 3.14: Spectrum of the solution obtained after centrifuging the reaction mixture obtained. In red, we have excitation curves ( $\text{em}=650\text{nm}$ ) and at black emission ( $\text{ex}=450\text{nm}$ ).

## 4 Stability test

Excision surgeries are long and can take hours. So when using fluorescence guided surgery, the dye will be irradiated for a long time and it cannot degrade and lose fluorescence properties. To prove our model, we performed a time base measurement of fluorescence with the free dye and Si5@FIGS. The fluorescence intensity was recorded at 800 nm for 5.6 hours, as a proof of concept for the better stability of the dye inside a particle (fig.3.15). The intensity values are not relevant since the values are proportional to concentration, and the incorporation of the dye inside the particles was not measured. [34]

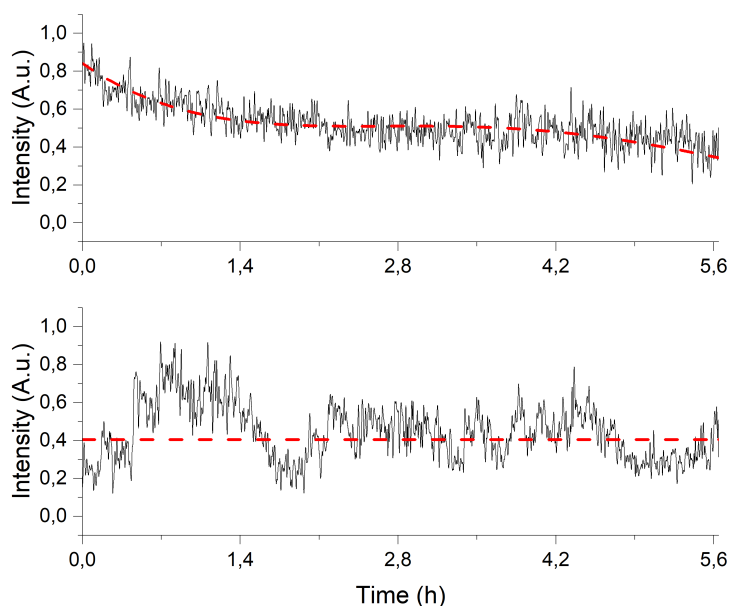


Figure 3.15: Fluorescence intensity at 800 nm with 680 nm excitation for free dye (a) and Si5@FIGS (b). Red lines are a guide to the eye.

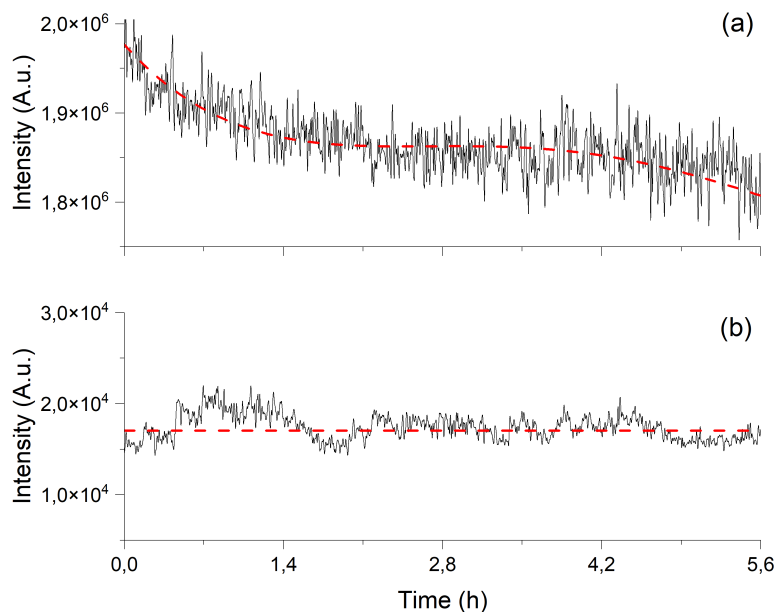


Figure 3.16: Fluorescence intensity at 800 nm with 680 nm excitation for free dye (a) and Si5@FIGS (b) with scales adapted for a better visualization.

There were some problems in the fluorolog lamp so there was a considerable amount of noise in each measurements. For a better understanding of the results, the scales of the graphs were adjusted in fig. 3.16. In free dye, there is a reduction in the fluorescence intensity during the 5.6 h of irradiation. In the particles almost no reduction is observed. This validates the photo-degradation protection offered by the silica matrix, due to the oxygen shielding effect. The presence of oxygen promotes the development of free radicals, mostly in the presence of UV or visible light. These interfere with the dye structure, attacking specially the double covalent bonds and aromatic moieties, leading to a lost of fluorescence. [35] We demonstrated that for at least 5.6 h we can have the nanoparticles irradiated without a significant loss of fluorescence intensity, being a great indicator for use in FGS.

## 5 Cell Viability

If the nanoparticles are going to be used in Fluorescence Guided Surgery (FGS), they cannot be toxic to human cells. To evaluate their toxicity, a cell viability test was performed. This determines the percentage of viable cells comparing to control (CTR, cells incubated with complete medium) by the following equation

$$\text{Cell viability}(\%) = \frac{OD_t}{OD_{CTR}} \times 100 \quad (3.1)$$

where  $OD_t$  is the optical density of the cells incubated with the tested formulations and  $OD_{CTR}$  is the optical density of control cells, corresponding to 100 % cell viability. The plate in test can be seen below (fig. 3.17). The first column works as a control with a concentration of 0  $\mu\text{g}$  of particles per mL of water, and moving to the right we have increasingly concentrations of SiNPs functionalized with folic acid (1.5 to 200  $\mu\text{g}/\text{mL}$ ).

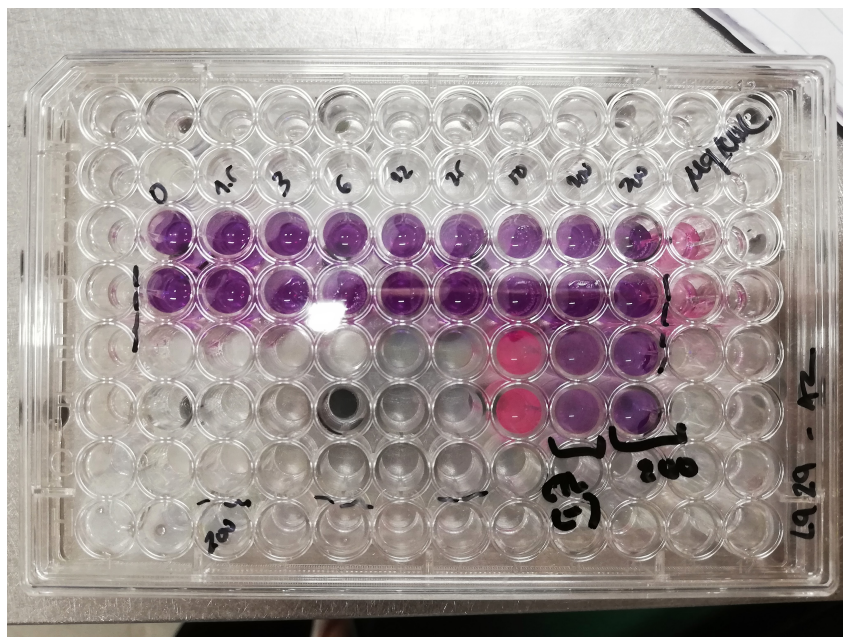


Figure 3.17: 96-Well Cell Culture Plate.

The colour changes from a purple-blue to red and this changes can be measured using fluorescence or absorbance measurements. [36] The pinker the colour and therefore higher counts, the more cells are viable. In Table 3.4, the results were measured one hour after the introduction of the particles and PrestoBlue™. In Table 3.5, the particles were added to the cells, and incubation was proceed for 48 h. PrestoBlue™ was then added, and the results measured one hour later. The results are graphically represented in fig. 3.18.

Table 3.4: Cell viability after 1 h of PrestoBlue™ introduction.

( $\mu\text{g/mL}$ )	0	1.5	3	6	12.5	25	50	100	200
<b>Counts</b>	23535	-	20882	20065	23143	20446	17950	19453	10647
<b>Cell Viability (%)</b>	100	-	88	84	98	86	74	82	42

Table 3.5: Cell viability after 48 h incubation.

( $\mu\text{g/mL}$ )	0	1.5	3	6	12.5	25	50	100	200
<b>Counts</b>	8224	8760	11379	12835	13553	12690	12660	7171	6666
<b>Cell Viability (%)</b>	100	108	146	168	178	166	165	85	77

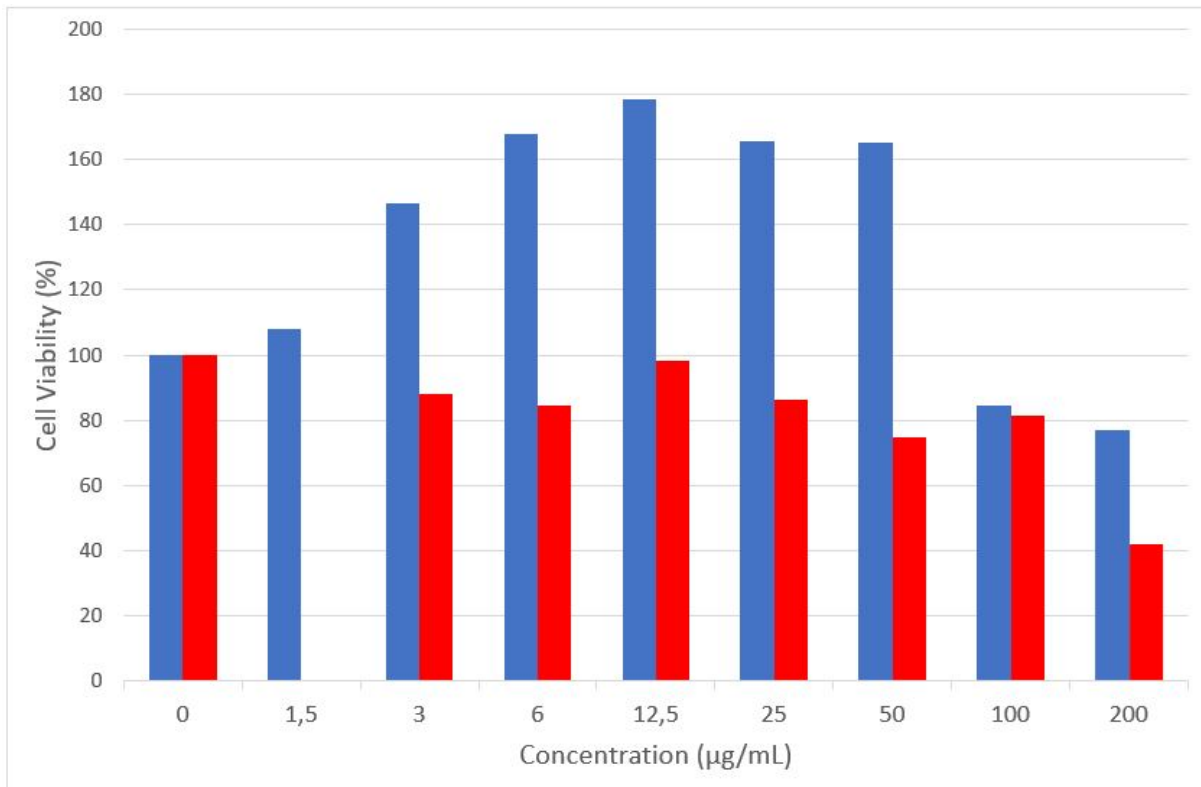


Figure 3.18: Graphic representation of cell viability after 1h of introduction of particles (red) and after 48h (blue).

Due to experimental errors, we have values higher than 100 %, that are easily explained by small differences in the number of cells added, and/or small variations in the volume of PrestoBlue™ added to each well.

In the concentration of 200 µg/mL, some precipitation was noticed, so it is clear to assume that this concentration was too high to be further used. Now looking at the cell viability, we can see that 100 and 200 µg/mL present some degree of toxicity to the cells, being the last one very significant. For the other values, we can say that the particles are biocompatible.



## Chapter 4

# Conclusions

In this work, silica nanoparticles were synthesized with an incorporated dye and functionalized with folic acid for better targeting. The synthesis itself presented no challenges being the sizes easily tailorable and resulting in monodispersed spherical particles.

The incorporation of the dye was proved by the fluorescence spectra, nevertheless the presence of unexpected peaks lead us to think that some degradation happened and a by-product was included in the matrix, since it remained in the particles even after washing. This sub-product is thought to be one of the constituent groups of the FIGS-IST-Dye1 obtained through degradation due to pH, but needs further investigation to elucidate the origin.

For the functionalization with folic acid, two processes were tested and quantified through NMR. The one step method resulted in unrealistic surface coverage values. The two step was then chosen for further synthesis, seeing that the surface coverage obtained is consistent with the quantification selected. The folic acid remained intact during the functionalization process and was successfully connected to the particles.

As a proof of concept for the particle oxygen shielding effect, a kinetics fluorescence study was performed. The particles and the free FIGS-IST-Dye1 were irradiated at 680 nm for 5.6 h, and the emission measured at the 800 nm. Over time, it was verified that the dye on its own had a reduction of intensity more significant than inside the particle. This reduction is associated with the photo-degradation of the structure, so the SiNP were proven to protect FIGS-IST-Dye1.

Finally, to ensure the biocompatibility, a cell viability test was performed. In general, the particles presented no toxicity to the cells. At concentrations superior to 100  $\mu\text{g/mL}$  that was no longer true. At 200  $\mu\text{g/mL}$ , we could also verify some precipitation in the well.

In conclusion, the goal of the thesis was successfully achieved. We were able to produce functional nanoparticles that are fluorescent under NIR light and with targeting groups for cancer cells. Further tests need to be done, first to confirm what was the sub-product obtained during the synthesis of SiNP with FIGS-IST-Dye1 and second, to prove the higher affinity and accumulation of the nanoparticles in the tumorous tissue. The quantum yield of the free dye and nanoparticles should also be measured to quantify if there is fluorescence improvement when incorporating into a particle.





# Bibliography

- [1] "Cancer Fact Sheet," Available at <https://www.who.int/news-room/fact-sheets/detail/cancer> [Accessed on 04/04/2021].
- [2] "How cancer starts, grows and spreads- Canadian Cancer Society," Available at <https://www.cancer.ca/en/cancer-information/cancer-101/what-is-cancer/how-cancer-starts-grows-and-spreads/?region=on> [Accessed on 24/05/2021].
- [3] "Definition of margin - NCI Dictionary of Cancer Terms - National Cancer Institute," Available at <https://www.cancer.gov/publications/dictionaries/cancer-terms/def/margin> [Accessed on 28/10/2021].
- [4] Y. Zheng, H. Yang, H. Wang, K. Kang, W. Zhang, G. Ma, and S. Du, "Fluorescence-guided surgery in cancer treatment: current status and future perspectives," *Annals of Translational Medicine*, pp. S6–S6, 2019.
- [5] T. M. Lwin, R. M. Hoffman, and M. Bouvet, "The development of fluorescence guided surgery for pancreatic cancer: from bench to clinic," *Expert Review of Anticancer Therapy*, pp. 651–662, 2018.
- [6] ThermoFisher Scientific, "Fluorescent Probes," Available at <https://www.thermofisher.com/pt/en/home/life-science/protein-biology/protein-biology-learning-center/protein-biology-resource-library/pierce-protein-methods/fluorescent-probes.html> [Accessed on 20/06/2021].
- [7] T. Ribeiro, S. Raja, A. S. Rodrigues, F. Fernandes, C. Baleizão, and J. P. S. Farinha, "NIR and visible peryleneimide-silica nanoparticles for laser scanning bioimaging," *Dyes and Pigments*, pp. 227–234, 2014.
- [8] T. Nagaya, Y. A. Nakamura, P. L. Choyke, and H. Kobayashi, "Fluorescence-guided surgery," *Frontiers in Oncology*, p. 314, 2017.
- [9] T. Mangeolle, I. Yakavets, S. Marchal, M. Debayle, T. Pons, L. Bezdetnaya, and F. Marchal, "Fluorescent nanoparticles for the guided surgery of ovarian peritoneal carcinomatosis," *Nanomaterials*, pp. 1–20, 2018.
- [10] J. F. Bringley, T. L. Penner, R. Wang, J. F. Harder, W. J. Harrison, and L. Buonemani, "Silica nanoparticles encapsulating near-infrared emissive cyanine dyes," *Journal of Colloid and Interface Science*, pp. 132–139, 2008.
- [11] H. Wongso, I. Mahendra, and A. Kurniawan, "Exploring the role of fluorescence image-guided surgery (FIGS) in surgical oncology (nuclear medicine)," *AIP Conference Proceedings*, p. 020108, 2021.
- [12] M. V. Marshall, D. Draney, E. M. Sevic-Muraca, and D. M. Olive, "Single-Dose Intravenous Toxicity Study of IRDye 800CW in Sprague-Dawley Rats," *Molecular Imaging and Biology*, pp. 583–594, 2010.

- [13] J. A. Carr, D. Franke, J. R. Caram, C. F. Perkinson, M. Saif, V. Askoxylakis, M. Datta, D. Fukumura, R. K. Jain, M. G. Bawendi, and O. T. Bruns, "Shortwave infrared fluorescence imaging with the clinically approved near-infrared dye indocyanine green," *Proceedings of the National Academy of Sciences*, pp. 4465–4470, 2018.
- [14] Li-Cor, "IRDye® 800CW Carboxylate NIR Dye Pack Insert," Available at <https://www.licor.com/bio/reagents/irdye-800cw-carboxylate> [Accessed on 14/10/2021].
- [15] T. Shukla, N. Upmanyu, S. P. Pandey, and M. S. Sudheesh, *Chapter 14 - Site-specific drug delivery, targeting, and gene therapy*, A. M. Grumezescu, Ed. William Andrew Publishing, 2019.
- [16] G. L. Zwicke, G. A. Mansoori, and C. J. Jeffery, "Utilizing the folate receptor for active targeting of cancer nanotherapeutics," *Nano Reviews*, p. 18496, 2012.
- [17] P. Foroozandeh and A. A. Aziz, "Insight into Cellular Uptake and Intracellular Trafficking of Nanoparticles," *Nanoscale Research Letters*, 2018. [Online]. Available: [/pmc/articles/PMC6202307//pmc/articles/PMC6202307/?report=abstracthttps://www.ncbi.nlm.nih.gov/pmc/articles/PMC6202307/](https://pubmed.ncbi.nlm.nih.gov/3622307/)
- [18] A. M. Santiago, "Biocompatible Hybrid Materials for Fluorescence Imaging Biodiagnostic Applications Biological Engineering Examination Committee," Ph.D. dissertation, IST, 2013.
- [19] M. Bansal, N. Singh, S. Pal, I. Dev, and K. M. Ansari, "Chemopreventive Role of Dietary Phytochemicals in Colorectal Cancer," *Advances in Molecular Toxicology*, pp. 69–121, 2018.
- [20] M. Benelmekki, "An introduction to nanoparticles and nanotechnology," *Designing Hybrid Nanoparticles*, pp. 1–14, 2015.
- [21] A. M. Santiago, T. Ribeiro, A. S. Rodrigues, B. Ribeiro, R. F. Frade, C. Baleizão, and J. P. S. Farinha, "Multifunctional Hybrid Silica Nanoparticles with a Fluorescent Core and Active Targeting Shell for Fluorescence Imaging Biodiagnostic Applications," *European Journal of Inorganic Chemistry*, pp. 4579–4587, 2015.
- [22] W. Stöber, A. Fink, and E. Bohn, "Controlled growth of monodisperse silica spheres in the micron size range," *Journal of Colloid and Interface Science*, pp. 62–69, 1968.
- [23] P. P. Ghimire and M. Jaroniec, "Renaissance of Stöber method for synthesis of colloidal particles: New developments and opportunities," *Journal of Colloid and Interface Science*, pp. 838–865, 2021.
- [24] S. Silva, A. Almeida, and N. Vale, "Combination of cell-penetrating peptides with nanoparticles for therapeutic application: A review," *Biomolecules*, 2019.
- [25] T. Ribeiro, S. Raja, A. S. Rodrigues, F. Fernandes, J. P. S. Farinha, and C. Baleizão, "High performance NIR fluorescent silica nanoparticles for bioimaging," *RSC Advances*, pp. 9171–9174, 2013.
- [26] Y. Luo and J. Lin, "Solvent induced different morphologies of bis(propyl)triethoxysilane substituted perylene diimide and their optical properties," *Journal of Colloid and Interface Science*, pp. 625–630, 2006.
- [27] M. Cabañas, D. Lozano, A. Torres-Pardo, C. Sobrino, J. González-Calbet, D. Arcos, and M. Vallet-Regí, "Features of aminopropyl modified mesoporous silica nanoparticles. Implications on the active targeting capability," *Materials Chemistry and Physics*, pp. 260–269, 2018.
- [28] E. Ortiz-Islas, A. Sosa-Arróniz, M. E. Manríquez-Ramírez, C. E. Rodríguez-Pérez, F. Tzompantzi, and J. M. Padilla, "Mesoporous silica nanoparticles functionalized with folic acid for targeted release Cis-Pt to glioblastoma cells," *Reviews on Advanced Materials Science*, pp. 25–37, 2021.

- [29] “Intensity - Volume - Number | Technical Notes Malvern Panalytical,” Available at [https://www.malvernpanalytical.com/en/learn/knowledge-center/technical-notes/TN101104IntensityVolumeNumber.html?utm\\_source=MaterialsTalks&utm\\_medium=blog&utm\\_campaign=null&utm\\_term=9612&utm\\_content=entryContentLink](https://www.malvernpanalytical.com/en/learn/knowledge-center/technical-notes/TN101104IntensityVolumeNumber.html?utm_source=MaterialsTalks&utm_medium=blog&utm_campaign=null&utm_term=9612&utm_content=entryContentLink) [Accessed on 18/10/2021].
- [30] “Dynamic Light Scattering (DLS) | Common Terms Defined | Malvern Panalytical,” Available at <https://www.malvernpanalytical.com/en/learn/knowledge-center/whitepapers/WP111214DLSTermsDefined> [Accessed on 18/10/2021].
- [31] “Carboxylic acid reactions overview | Khan Academy,” Available at <https://www.khanacademy.org/test-prep/mcat/chemical-processes/carboxylic-acids/a/carboxylic-acid-reactions-overview> [Accessed on 14/10/2021].
- [32] C. I. C. Crucho, C. Baleizão, and J. P. S. Farinha, “Functional Group Coverage and Conversion Quantification in Nanostructured Silica by  $^1\text{H}$  NMR,” *Analytical Chemistry*, pp. 681–687, 2017.
- [33] “Perylene-diimide, [PDI],” Available at <https://omlc.org/spectra/PhotochemCAD/html/143.html> [Accessed on 26/10/2021].
- [34] H. Itagaki, “Fluorescence Spectroscopy,” in *Experimental Methods in Polymer Science: Modern Methods in Polymer Research and Technology*. Academic Press, 2000, pp. 155–260.
- [35] B. R. Hammond, B. A. Johnson, and E. R. George, “Oxidative photodegradation of ocular tissues: Beneficial effects of filtering and exogenous antioxidants,” *Experimental Eye Research*, pp. 135–150, 2014.
- [36] “PrestoBlue™ Cell Viability Reagent,” Available at <https://www.thermofisher.com/order/catalog/product/A13261> [Accessed on 30/10/2021].



# Appendix

## A) DLS Correlograms

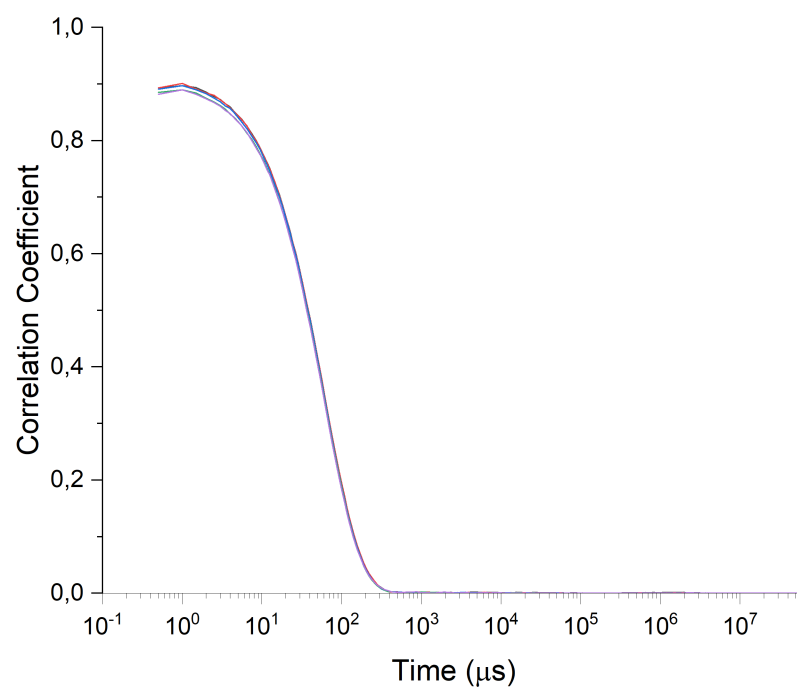


Figure 1: Correlograms obtained by DLS for Si4@PDI.

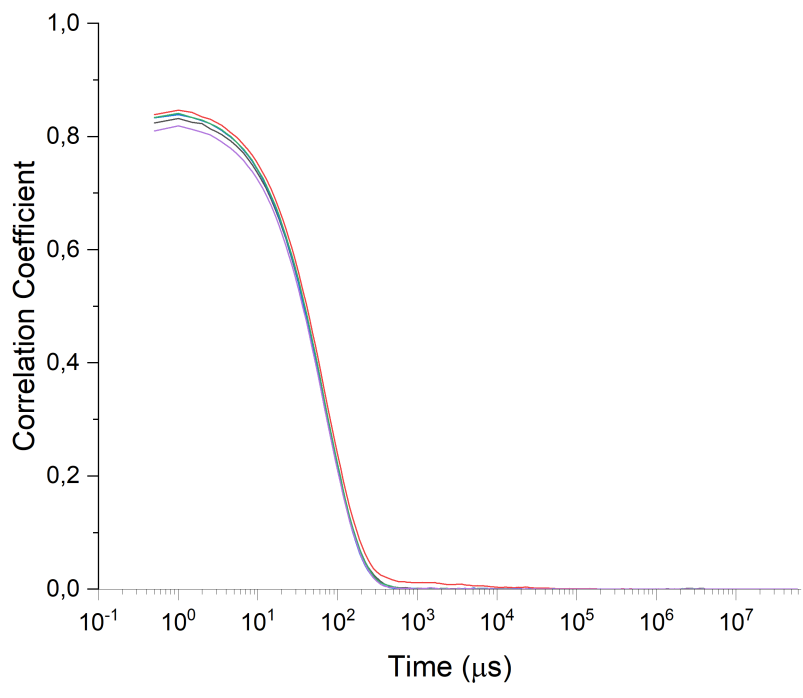


Figure 2: Correlograms obtained by DLS for Si5@FIGS.

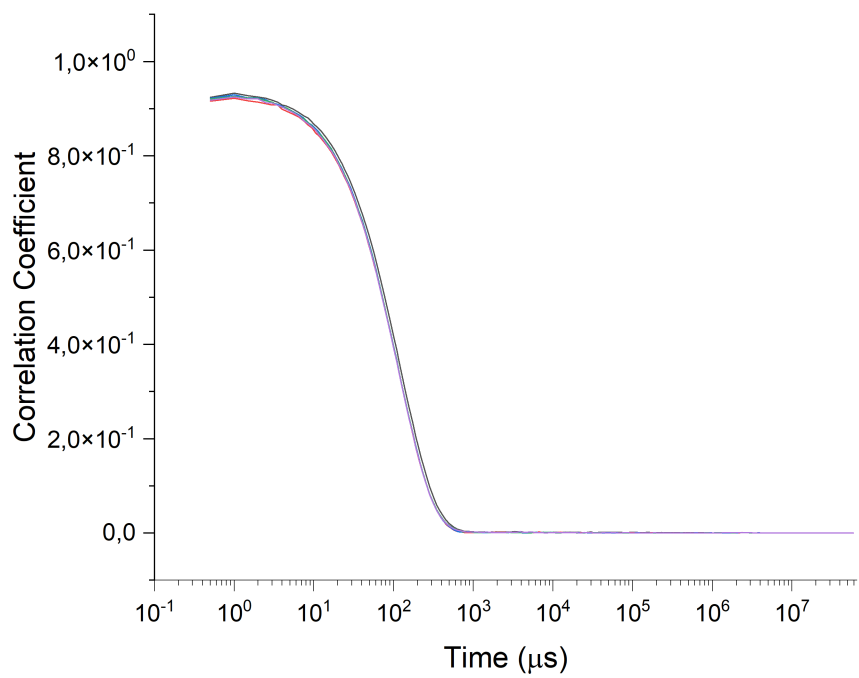


Figure 3: Correlograms obtained by DLS for Si6A.

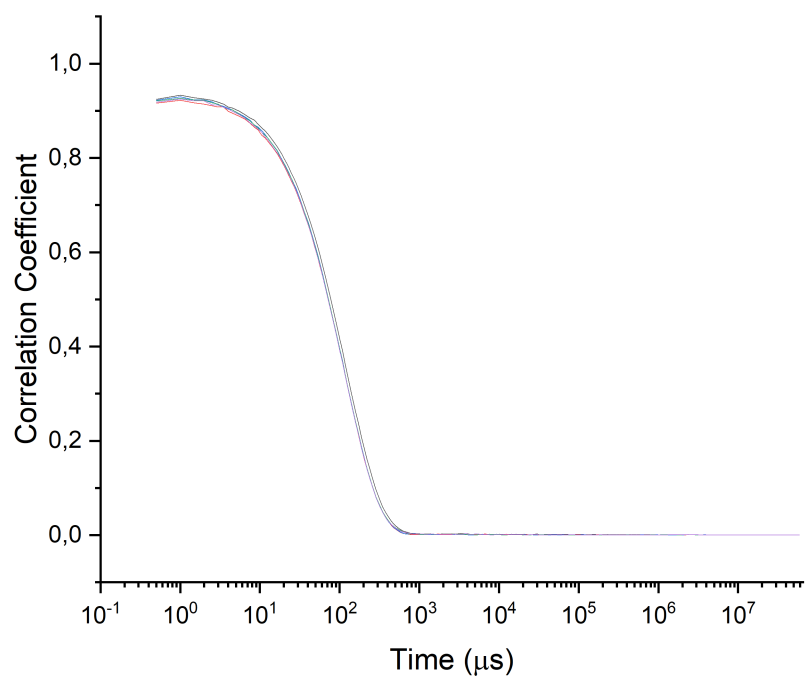


Figure 4: Correlograms obtained by DLS for Si6B.

## B) NMR spectra

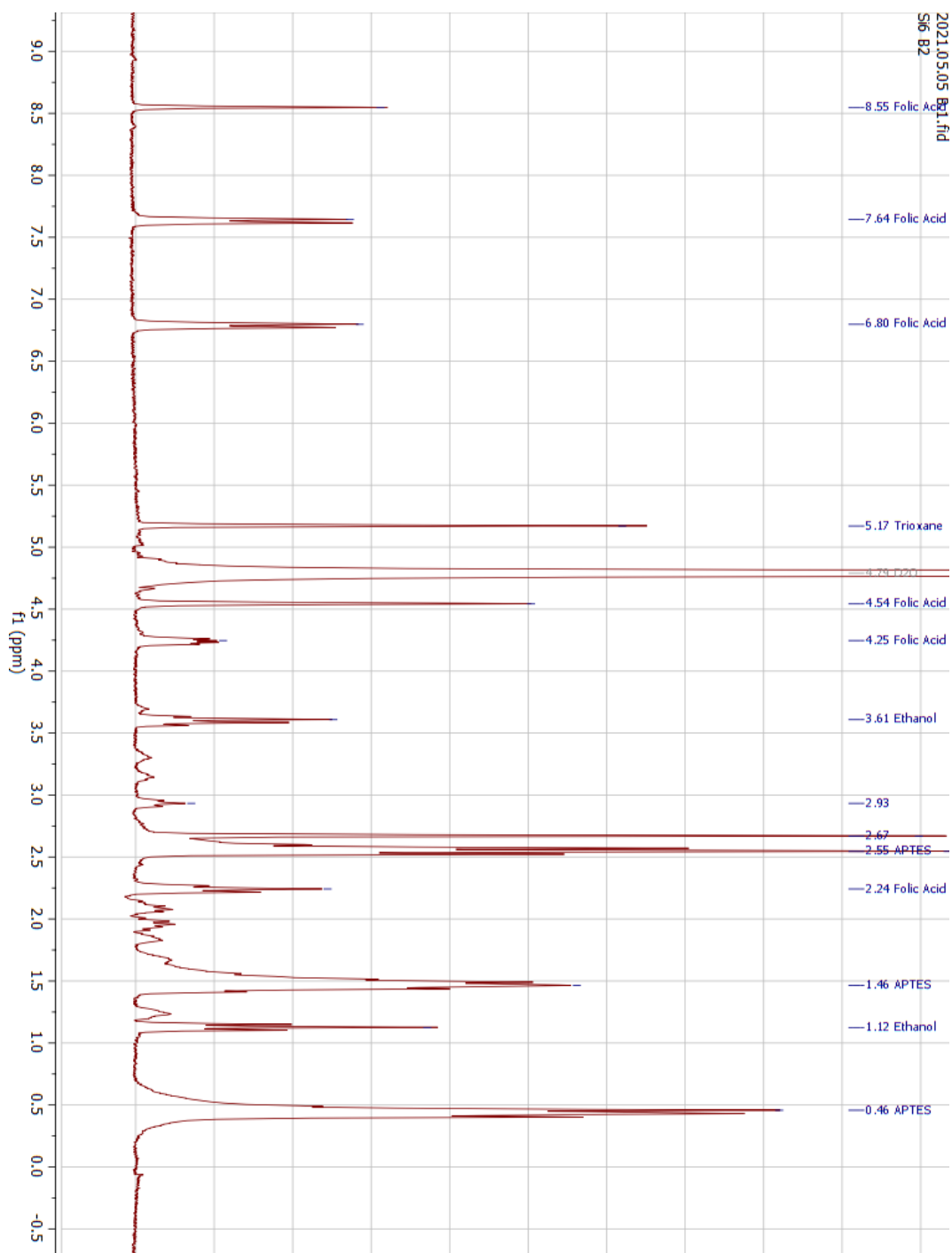


Figure 5:  $^1H$  NMR of Si-PDI functionalized by the One Step method. Peak assignment: 8.55, 7.64, 6.80 Folic Acid; 5.17 Trioxane; 4.79 D2O; 3.61, 1.12 Ethanol; 2.55, 1.46, 0.46 APTES.



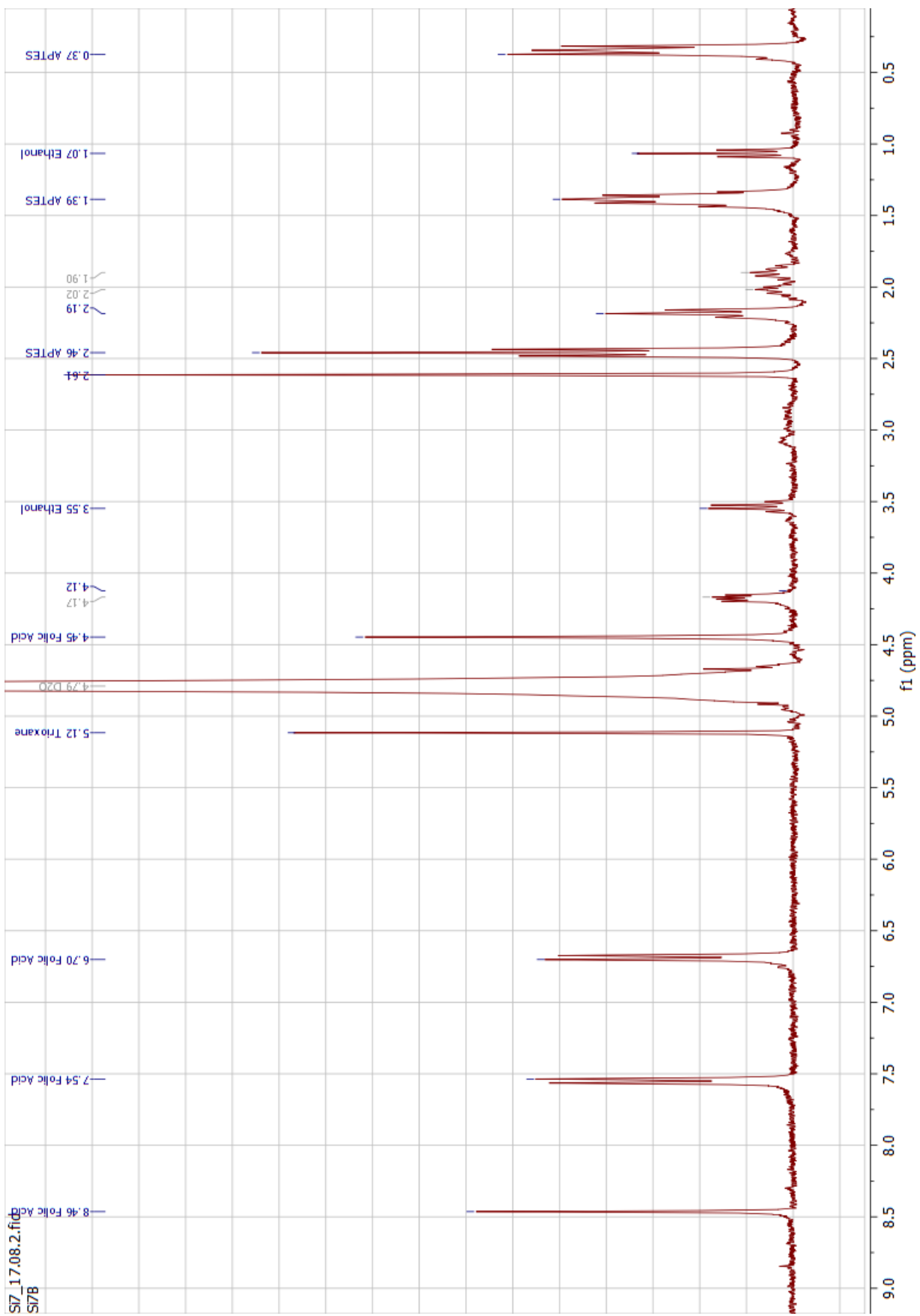


Figure 6:  $^1\text{H}$  NMR of S14-PDI functionalized by the One Step method. Peak assignment: 8.46, 7.54, 6.70 Folic Acid; 5.12 Trioxane; 4.79 D2O; 3.55, 1.07 Ethanol; 2.46, 1.39, 0.37 APTES.

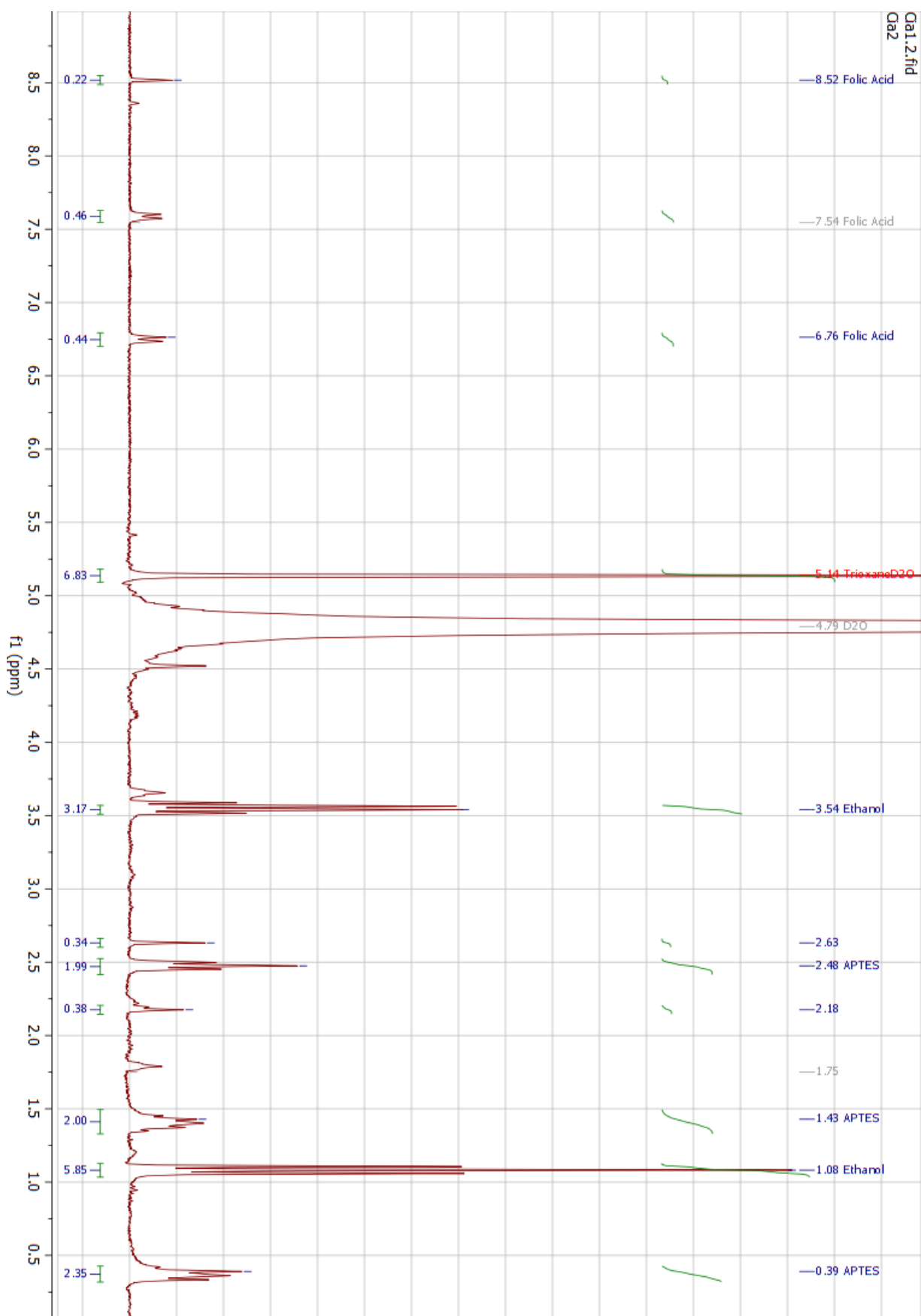


Figure 7:  $^1H$  NMR of Si5-FIGS-IST-Dye1 functionalized by the Two Step method, with integration ranges represented. Peak assignment: 8.52, 7.54, 6.76 Folic Acid; 5.14 Trioxane; 4.79 D2O; 3.54, 1.08 Ethanol; 2.48, 1.43, 0.39 APTES.